1-1-2020

Full orbital solution for the binary system in the northern Galactic disc microlensing event Gaia16aye

Wyrzykowski
Uniwersytet Warszawski

P. Mróz
Uniwersytet Warszawski

K. A. Rybicki
Uniwersytet Warszawski

M. Gromadzki
Uniwersytet Warszawski

Z. Kołaczkowski
University of Wroclaw

See next page for additional authors

Recommended Citation

Wyrzykowski., Mróz, P., Rybicki, K., Gromadzki, M., Kołaczkowski, Z., Zieliński, M., Zieliński, P., Britavskiy, N., Gomboc, A., Sokolovsky, K., Hodgkin, S., Abe, L., Aldi, G., Almannaei, A., Altavilla, G., Al Qasim, A., Anupama, G., Awiphan, S., Bachelet, E., Baklş, V., Baker, S., Bartlett, S., Bendjoya, P., Benson, K., Bikmaev, I., Birenbaum, G., Blagorodnova, N., Blanco-Cuaresma, S., Boeva, S., Bonanos, A., Bozza, V., Bramich, D., & Bruni, I. (2020). Full orbital solution for the binary system in the northern Galactic disc microlensing event Gaia16aye. *Astronomy and Astrophysics, 633* https://doi.org/10.1051/0004-6361/201935097

Authors

Wyrzykowski, P. Mróz, K. A. Rybicki, M. Gromadzki, Z. Kołaczkowski, M. Zieliński, P. Zieliński, N. Britavskiy, A. Gomboc, K. Sokolovsky, S. T. Hodgkin, L. Abe, G. F. Aldi, A. Almannaei, G. Altavilla, A. Al Qasim, G. C. Anupama, S. Awiphan, E. Bachelet, V. Baklş, S. Baker, S. Bartlett, P. Bendjoya, K. Benson, I. F. Bikmaev, G. Birenbaum, N. Blagorodnova, S. Blanco-Cuaresma, S. Boeva, A. Z. Bonanos, V. Bozza, D. M. Bramich, and I. Bruni

A&A 633, A98 (2020)
https://doi.org/10.1051/0004-6361/201935097

Astronomy & Astrophysics

Full orbital solution for the binary system in the northern Galactic disc microlensing event Gaia16aye[⋆]

Ł. Wyrzykowski[1], P. Mróz[1], K. A. Rybicki[1], M. Gromadzki[1], Z. Kołaczkowski[44,78,†], M. Zieliński[1], P. Zieliński[1], N. Britavskiy[4,5], A. Gomboc[34], K. Sokolovsky[18,3,65], S. T. Hodgkin[6], L. Abe[88], G. F. Aldi[19,79], A. AlMannaei[61,99], G. Altavilla[71,7], A. Al Qasim[61,99], G. C. Anupama[8], S. Awiphan[9], E. Bachelet[62], V. Bakış[10], S. Baker[99], S. Bartlett[49], P. Bendjoya[11], K. Benson[99], I. F. Bikmaev[75,86], G. Birenbaum[12], N. Blagorodnova[23], S. Blanco-Cuaresma[14,73], S. Boeva[15], A. Z. Bonanos[18], V. Bozza[19,79], D. M. Bramich[61], I. Bruni[24], R. A. Burenin[83,84], U. Burgaz[20], T. Butterley[21], H. E. Caines[33], D. B. Caton[92], S. Calchi Novati[82], J. M. Carrasco[22], A. Cassan[28], V. Čepas[55], M. Cropper[99], M. Chruślińska[1,23], G. Clementini[24], A. Clerici[34], D. Conti[90], M. Conti[47], S. Cross[62], F. Cusano[24], G. Damljanovic[25], A. Dapergolas[18], G. D'Ago[80], J. H. J. de Bruijne[26], M. Dennefeld[28], V. S. Dhillon[29,4], M. Dominik[30], J. Dziedzic[1], O. Erece[31], M. V. Eselevich[85], H. Esenoglu[32], L. Eyer[73], R. Figuera Jaimes[30,52], S. J. Fossey[33], A. I. Galeev[75,86], S. A. Grebenev[83], A. C. Gupta[98], A. G. Gutaev[75], N. Hallakoun[12], A. Hamanowicz[1,35], C. Han[2], B. Handzlik[36], J. B. Haislip[93], L. Hanlon[101], L. K. Hardy[29], D. L. Harrison[6,87], H. J. van Heerden[102], V. L. Hoette[94], K. Horne[30], R. Hudec[38,75,39], M. Hundertmark[40], N. Ihanec[34], E. N. Irtuganov[75,86], R. Itoh[42], P. Iwanek[1], M. D. Jovanovic[25], R. Janulis[55], M. Jelínek[38], E. Jensen[91], Z. Kaczmarek[1], D. Katz[100], I. M. Khamitov[43,75], Y. Kilic[31], J. Klencki[1,23], U. Kolb[46], G. Kopacki[44], V. V. Kouprianov[93], K. Kruszyńska[1], S. Kurowski[36], G. Latev[15], C.-H. Lee[16,17], S. Leonini[47], G. Leto[48], F. Lewis[49,58], Z. Li[62], A. Liakos[18], S. P. Littlefair[29], J. Lu[50], C. J. Manser[51], S. Mao[52], D. Maoz[12], A. Martin-Carrillo[101], J. P. Marais[102], M. Maskoliūnas[55], J. R. Maund[29], P. J. Meintjes[102], S. S. Melnikov[75,86], K. Ment[40], P. Mikołajczyk[44], M. Morrell[46], N. Mowlavi[73], D. Moździerski[44], D. Murphy[101], S. Nazarov[89], H. Netzel[1,78], R. Nesci[66], C.-C. Ngeow[53], A. J. Norton[46], E. O. Ofek[54], E. Pakštienė[55], L. Palaversa[6,73], A. Pandey[98], E. Paraskeva[18,77], M. Pawlak[1,64], M. T. Penny[56], B. E. Penprase[57], A. Piascik[58], J. L. Prieto [95,96], J. K. T. Qvam[97], C. Ranc[69], A. Rebassa-Mansergas[59,70], D. E. Reichart[93], P. Reig[60,74], L. Rhodes[29], J.-P. Rivet[88], G. Rixon[6], D. Roberts[46], P. Rosi[47], D. M. Russell[61], R. Zanmar Sanchez[48], G. Scarpetta[19,81], G. Seabroke[99], B. J. Shappee[68], R. Schmidt[40], Y. Shvartzvald[13,⋆⋆], M. Sitek[1], J. Skowron[1], M. Śniegowska[1,76,78], C. Snodgrass[45], P. S. Soares[33], B. van Soelen[102], Z. T. Spetsieri[18,77], A. Stankevičiūtė[1], I. A. Steele[58], R. A. Street[62], J. Strobl[38], E. Strubble[94], H. Szegedi[102], L. M. Tinjaca Ramirez[47], L. Tomasella[63], Y. Tsapras[40], D. Vernet[11], S. Villanueva Jr.[56], O. Vince[25], J. Wambsganss[40,41], I. P. van der Westhuizen[102], K. Wiersema[51,67], D. Wium[102], R. W. Wilson[21], A. Yoldas[6], R. Ya. Zhuchkov[75,86], D. G. Zhukov[75], J. Zdanavičius[55], S. Zoła[36,37], and A. Zubareva[72,3]

(Affiliations can be found after the references)

Received 22 January 2019 / Accepted 10 October 2019

ABSTRACT

Gaia16aye was a binary microlensing event discovered in the direction towards the northern Galactic disc and was one of the first microlensing events detected and alerted to by the *Gaia* space mission. Its light curve exhibited five distinct brightening episodes, reaching up to $I = 12$ mag, and it was covered in great detail with almost 25 000 data points gathered by a network of telescopes. We present the photometric and spectroscopic follow-up covering 500 days of the event evolution. We employed a full Keplerian binary orbit microlensing model combined with the motion of Earth and *Gaia* around the Sun to reproduce the complex light curve. The photometric data allowed us to solve the microlensing event entirely and to derive the complete and unique set of orbital parameters of the binary lensing system. We also report on the detection of the first-ever microlensing space-parallax between the Earth and *Gaia* located at L2. The properties of the binary system were derived from microlensing parameters, and we found that the system is composed of two main-sequence stars with masses $0.57 \pm 0.05\, M_\odot$ and $0.36 \pm 0.03\, M_\odot$ at 780 pc, with an orbital period of 2.88 years and an eccentricity of 0.30. We also predict the astrometric microlensing signal for this binary lens as it will be seen by *Gaia* as well as the radial velocity curve for the binary system. Events such as Gaia16aye indicate the potential for the microlensing method of probing the mass function of dark objects, including black holes, in directions other than that of the Galactic bulge. This case also emphasises the importance of long-term time-domain coordinated observations that can be made with a network of heterogeneous telescopes.

Key words. gravitational lensing: micro – techniques: photometric – binaries: general – stars: individual: Gaia16aye-L

1. Introduction

Measuring the masses of stars or stellar remnants is one of the most challenging tasks in modern astronomy. Binary systems were the first to facilitate mass measurement through the Doppler effect in radial velocity measurements (e.g. Popper 1967), leading to the mass-luminosity relation and an advancement in the understanding of stellar evolution (e.g. Paczyński 1971; Pietrzyński et al. 2010). However, these techniques require the binary components to emit detectable amounts of light, often demanding large-aperture telescopes and sensitive instruments. In order to study the invisible objects, in particular stellar remnants such as neutron stars or black holes, other means of mass measurement are necessary. Recently, the masses of black holes

⋆ Full Tables B.1–D.1 are only available at the CDS via anonymous ftp to cdsarc.u-strasbg.fr (130.79.128.5) or via http://cdsarc.u-strasbg.fr/viz-bin/cat/J/A+A/633/A98

⋆⋆ NASA Postdoctoral Program Fellow.

† Deceased.

were measured when a close binary system tightened its orbit and emitted gravitational waves (e.g. Abbott et al. 2016), yielding unexpectedly high masses that were not observed before (e.g. Abbott et al. 2017; Belczynski et al. 2016; Bird et al. 2016). Because of the low merger rates, gravitational wave experiment detections are limited to very distant galaxies. Other means of mass measurement are therefore required to probe the faint and invisible populations in the Milky Way and its vicinity.

Gravitational microlensing allows for detection and study of binary systems regardless of the amount of light they emit and regardless of the radial velocities of the components, as long as the binary crosses the line of sight to a star that is bright enough to be observed. Therefore, this method offers an opportunity to detect binary systems that contain planets (e.g. Gould & Loeb 1992; Albrow et al. 1998; Bond et al. 2004; Udalski et al. 2005), planets orbiting a binary system of stars (e.g. Poleski et al. 2014; Bennett et al. 2016), and black holes or other dark stellar remnants (e.g. Shvartzvald et al. 2015).

Typically, searches for microlensing events are conducted in the direction of the Galactic bulge because of the high stellar density, potential sources and lenses, and the high microlensing optical depth (e.g. Kiraga & Paczynski 1994; Udalski et al. 1994a, 2015a; Paczynski 1996; Wozniak et al. 2001; Sumi et al. 2013; Wyrzykowski et al. 2015; Mróz et al. 2017). The regions of the Galactic plane outside of the bulge have occasionally also been monitored in the past for microlensing events, however, even though the predicted rates of events were orders of magnitude lower (e.g. Han 2008; Gaudi et al. 2008). Derue et al. (2001) first published microlensing events that were detected during the long-term monitoring of the selected disc fields. Two serendipitous discoveries of bright microlensing events outside of the bulge were reported by amateur observers, the Tago event (Fukui et al. 2007; Gaudi et al. 2008), and the Kojima-1 event (Nucita et al. 2018; Dong et al. 2019; Fukui et al. 2019), which has a signature of a planet next to the lens. The first binary microlensing event in the Galactic disc was reported in Rahal et al. (2009) (GSA14), but its light curve was too poorly sampled in order to conclude on the parameters of the binary lens.

The best-sampled light curves come from bulge surveys, such as MACHO (Alcock et al. 1997; Popowski et al. 2000), the Expérience pour la Recherche d'Objets Sombres (EROS; Hamadache et al. 2006), the Optical Gravitational Lensing Experiment (OGLE; Udalski et al. 1994a, 2000, 2015a), the Microlensing Observations in Astrophysics (MOA; Yock 1998; Sumi et al. 2013), and the Korean Microlensing Telescope Network (KMNet; Kim et al. 2016). In particular, the OGLE project has been monitoring the Galactic bulge regularly since 1992 and was the first to report on a binary microlensing event in 1993 (Udalski et al. 1994b). Binary microlensing events constitute about 10% of all events reported by the microlensing surveys of the bulge. The binary lens differs from a single lens when the component separation on the sky is of order of their Einstein radius Paczynski (1996) and Gould (2000), which is computed as

$$\theta_{\rm E} = \sqrt{\kappa M_L(\pi_{\rm l} - \pi_{\rm s})}, \ \kappa \equiv \frac{4G}{c^2} \approx 8.144 \,{\rm mas}\, M_\odot^{-1}, \quad (1)$$

where M_L is the total mass of the binary and $\pi_{\rm l}$ and $\pi_{\rm s}$ are parallaxes of the lens and the source, respectively. For the conditions in the Galaxy and a typical mass of the lens, the size of the Einstein ring is about 1 milliarcsecond (1 mas). Instead of a circular Einstein ring as in the case of a single lens (or very tight binary system), two (or more) lensing objects produce a complex curve on the sky, shaped by the mass ratio and projected separation of the components. This is called the critical curve. In the source plane this curve turns into a caustic curve (as opposed to a point in the case of a single lens), which denotes the places where the source is infinitely amplificated (e.g. Bozza 2001; Rattenbury 2009). As the source and the binary lens move, their relative proper motion changes the position of the source with respect to the caustics. Depending on this position, there are three (when the source is outside of the caustic) or five (inside the caustic) images of the source. Images also change their location as well as their size, therefore the combined light of the images we observe changes the observed amplification, with the most dramatic changes at the caustic crossings. In a typical binary lensing event the source–lens trajectory can be approximated with a straight line (e.g. Jaroszynski et al. 2004; Skowron et al. 2007). If the line crosses the caustic, it produces a characteristic U-shaped light curve because the amplification increases steeply as the source approaches the caustic and remains high inside the caustic (e.g. Witt & Mao 1995). If the source approaches one of the caustic cusps, the light curve shows a smooth increase, similar to a single lensing event. Identifying all these features in the light curve helps constrain the shape of the caustic and hence the parameters of the binary. An additional annual parallax effect causes the trajectory of the source to curve, which probes the caustic shape at multiple locations (e.g. An & Gould 2001; Skowron et al. 2009; Udalski et al. 2018) and thus helps constrain the solution of the binary system better.

The situation becomes more complex when a binary system rotates while lensing, which causes the binary configuration on the sky to change. This in turn changes the shape and size of the caustic (Albrow et al. 2000). In the case of most binary microlensing events the effect of the orbital motion can be neglected because the orbital periods are often much longer (typically years) than the duration of the event (typically weeks). However, in longer events the orbital motion has to be taken into account in the model. Together with the source–lens relative motion and the parallax effect, this causes the observed amplification to vary significantly during the event and may generate multiple crossings of the caustic and amplification due to cusp approach (e.g. Skowron et al. 2009). However, in rare cases, such a complex event allows us not only to measure the mass and distance of the lens, but also to derive all orbital parameters of the binary. The first such case was found by the OGLE survey in the event OGLE-2009-BLG-020 (Skowron et al. 2011), and its orbital parameters found in the model were verified with radial velocity measurement (Yee et al. 2016). The orbital motion was also modelled in the MOA-2011-BLG-090 and OGLE-2011-BLG-0417 events (Shin et al. 2012), but the former was too faint and the latter was not confirmed with radial velocity data (Boisse et al. 2015; Bachelet et al. 2018).

Additional information that helps constrain the parameters of the system may also come from space parallax (e.g. Refsdal 1966; Gould 1992; Gould et al. 2009). This is now being routinely done by observing microlensing events from the Earth and *Spitzer* or *Kepler*, separated by more than 1 au (e.g. Udalski et al. 2015b; Yee et al. 2015; Calchi Novati & Scarpetta 2016; Shvartzvald et al. 2016; Zhu et al. 2016; Poleski et al. 2016).

The most difficult parameter to measure, however, is the size of the Einstein radius. It can be found when the finite source effects are detected, when the angular source size is large enough to experience a significant gradient in the magnification near the centre of the Einstein ring or the binary lens caustic (e.g. Yoo et al. 2004; Zub et al. 2011). The measurement of the angular separation between the luminous lens and the source years or decades after the event also directly leads to calculation of

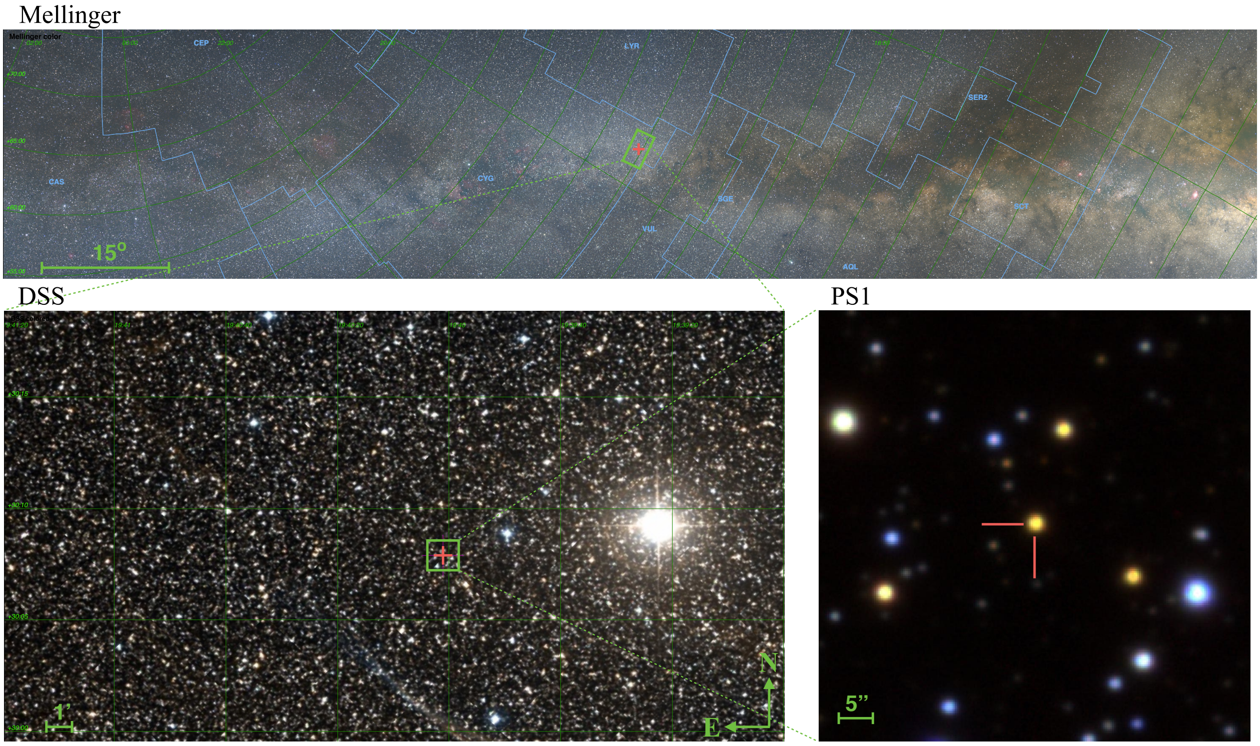

Fig. 1. Location of Gaia16aye on the sky. Images from Mellinger and DSS were obtained using the Aladin tool.

θ_E (e.g. Kozłowski et al. 2007). Otherwise, for dark lenses, the measurement of θ_E can only come from astrometric microlensing (Dominik & Sahu 2000; Belokurov & Evans 2002; Lu et al. 2016; Kains et al. 2017; Sahu et al. 2017). As shown in Rybicki et al. (2018), *Gaia* will soon provide precise astrometric observations for microlensing events, which will allow us to measure θ_E, but only for events brighter than about $V < 15$ mag.

Here we present Gaia16aye, a unique event from the Galactic disc, far from the Galactic bulge, which lasted almost two years and exhibited effects of binary lens rotation, an annual and space parallax, and a finite source. The very densely sampled light curve was obtained solely thanks to an early alert from *Gaia* and a dedicated ground-based follow-up of tens of observers, including amateurs and school pupils. The wealth of photometric data allowed us to find the unique solution for the binary system parameters.

The paper is organised as follows. Sections 2 and 3 describe the history of the detection and the photometric and spectroscopic data collected during the follow-up of Gaia16aye. In Sect. 4 we describe the microlensing model we used to reproduce the data. We then discuss the results in Sect. 5.

2. Discovery and follow-up of Gaia16aye

Gaia16aye was found during the regular examination of the photometric data collected by the *Gaia* mission. *Gaia* is a space mission of the European Space Agency (ESA) in science operation since 2014. Its main goal is to collect high-precision astrometric data, that is, positions, proper motions, and parallaxes, of all stars on the sky down to about 20.7 mag in *Gaia G* band (Gaia Collaboration 2016; Evans et al. 2018). While *Gaia* scans the sky multiple times, it provides near-real-time photometric data, which can be used to detect unexpected changes in the brightness or appearance of new objects from all over the sky. This is dealt with by the *Gaia* Science Alerts system (Wyrzykowski & Hodgkin 2012; Hodgkin et al. 2013; Wyrzykowski et al. 2014), which processes daily portions of the spacecraft data and produces alerts on potentially interesting transients. The main purpose of the publication of the alerts from *Gaia* is to enable the astronomical community to study the unexpected and temporary events. Photometric follow-up is necessary in particular in the case of microlensing events in order to fill the gaps between *Gaia* observations and subsequently construct a densely sampled light curve, sensitive to short-lived anomalies and deviations to the standard microlensing evolution (e.g. Wyrzykowski et al. 2012).

Gaia16aye was identified as an alert in the data chunk from 5 August 2016, processed on 8 August by the *Gaia* Science Alerts pipeline (*AlertPipe*), and published on *Gaia* Science Alerts webpages[1] on 9 August 2016, 10:45 GMT. The full *Gaia* photometry of Gaia16aye is listed in Table B.1.

The alert was triggered by a significant change in brightness of an otherwise constant-brightness star with $G = 15.51$ mag. The star has a counterpart in the 2MASS catalogue as 2MASS19400112+3007533 at RA, Dec (J2000.0) = 19:40:01.14, 30:07:53.36, and its source Id in *Gaia* DR2 is 2032454944878107008 (Gaia Collaboration 2018). Its Galactic coordinates are l,b = 64.999872, 3.839052 deg, which locates Gaia16aye well in the northern part of the Galactic Plane towards the Cygnus constellation (see Fig. 1).

Gaia collected its first observation of this star in October 2014, and until the alert in August 2016, there were no significant brightness variation in its light curve. Additionally, this part of the sky was observed prior to *Gaia* in 2011–2013 as part of a Nova Patrol (Sokolovsky et al. 2014), and no previous brightenings were detected at a limiting magnitude of $V \approx 14.2$.

In the case of Gaia16aye the follow-up was initiated because the source at its baseline was relatively bright and easily

[1] http://gsaweb.ast.cam.ac.uk/alerts/alert/Gaia16aye

accessible for a broad range of telescopes with smaller apertures. Moreover, microlensing events brighter than about $G = 16$ mag will have *Gaia* astrometric data of sufficient accuracy in order to detect the astrometric microlensing signal (Rybicki et al. 2018). For this purpose, we have organised a network of volunteering telescopes and observers who respond to *Gaia* alerts, in particular to microlensing event candidates, and invest their observing time to provide dense coverage of the light curve. The network is arranged under the Time-Domain work package of the European Commission's Optical Infrared Coordination Network for Astronomy (OPTICON) grant[2].

The follow-up observations started immediately after the announcement of the alert (the list of telescopes and their acronyms is provided in Table 1), with the first data points taken on the night 9/10 Aug. 2016 with the 0.6 m Akdeniz Univ. UBT60 telescope in the TUBITAK National Observatory, Antalya, the SAI Southern Station in Crimea, the pt5m telescope at the Roque de los Muchachos Observatory on La Palma (Hardy et al. 2015), the 0.8m Telescopi *Joan Oró* (TJO) at l'Observatori Astronomic del Montsec, and the 0.8 m robotic APT2 telescope in Serra La Nave (Catania). The data showed a curious evolution and a gradual rise (0.1 mag day^{-1}) in the light curve without change in colour, which is atypical for many known types of variable and cataclysmic variable stars. On the night 13/14 Aug. 2016 (HJD′ ≡ HJD-2450000.0 ~ 7614.5) the object reached a peak $V = 13.8$ mag ($B - V = 1.6$ mag, $I = 12.2$ mag), as detected by ATP2 and TJO, which was followed by a sudden drop by about 2 mag. Alerted by the unusual shape of the light curve, we obtained spectra of Gaia16aye with the 1.22 m Asiago telescope on 11 August and with the 2.0 m Liverpool Telescope (LT, La Palma) on 12 August, which were consistent with a normal K8-M2 type star (Bakis et al. 2016). The stellar spectra along with the shape of the light curve implied that Gaia16aye was a binary microlensing event, which was detected by *Gaia* at its plateau between the two caustic crossings, and we have observed the caustic exit with clear signatures of the finite source effects.

The continued follow-up after the first caustic exit revealed a very slow gradual rise in brightness (around 0.1 mag in a month). On 17 September 2016, it increased sharply by 2 mag (first spotted by the APT2 telescope), indicating the second caustic entry. The caustic crossing again showed a broad and long-lasting effect of finite source size (flattened peak), lasting for nearly 48 h between HJD′ = 7649.4 and 7651.4 and reaching about $V = 13.6$ mag and $I = 12$ mag. The caustic crossing was densely covered by the Liverpool Telescope and the 0.6 m Ostrowik Observatory near Warsaw, Poland.

Following the second caustic entry, the object remained very bright ($I \sim 12-14$ mag) and was observed by multiple telescopes from around the globe, both photometrically and spectroscopically. The complete list of telescopes and instruments involved in the follow-up observations of Gaia16aye is shown in Table 1, and their parameters are gathered in Table A.1. In total, more than 25 000 photometric and more than 20 spectroscopic observations were taken over the period of about two years. In early November 2016, the brightness trend changed from falling to rising, as expected for binary events during the caustic crossing (Nesci 2016; Khamitov et al. 2016a). A simple preliminary model for the binary microlensing event predicted the caustic exit to occur around November 20.8 UT (HJD′ = 7713.3) and the caustic crossing to last about seven hours (Mroz et al. 2016). In order to catch and cover the caustic exit well, an intensive observing campaign was begun, involving also amateur astronomical associations (including the British Astronomical Association and the German Haus der Astronomie) and school pupils. The observations were also reported live on Twitter (hashtag #Gaia16aye). A DDT observing time was allocated at the *William Herschel* Telescope (WHT/ACAM) and the Telescopio Nazionale *Galileo* (TNG/DOLORES) to provide low- and high-resolution spectroscopy at times close to the peak. However, the actual peak occurred about 20 h later than expected, on 21 November 16 UT (7714.17), and was followed by TRT-GAO, Aries130, CrAO, AUT25, T60, T100, RTT150 (detection of the fourth caustic was reported in Khamitov et al. 2016b), Montarrenti, Bialkow, Ostrowik, Krakow50, OndrejovD50, LT, pt5m, Salerno, and UCLO, spanning the whole globe, which provided 24-h coverage of the caustic exit. The sequence of spectroscopic observations before and at the very peak was taken with the IDS instrument on the *Isaac Newton* Telescope (INT). After the peak at 11.85 mag in I band, the event brightness smoothly declined, as caught by Swarthmore24, DEMONEXT, and AAVSO. The first datapoint taken on the next night from India (Aries130 telescope) showed $I = 14.33$ mag, indicating the complete exit from the caustic. The event then again began to rise very slowly, with a rate of 1 mag over four months, and it exhibited a smooth peak on 5 May 2017 (HJD′ = 7878), reaching $I = 13.3$ mag ($G \sim 14$ mag) (Wyrzykowski et al. 2017). After this, the light curve declined slowly and reached the pre-alert level in November 2017, at $G = 15.5$ mag. We continued our photometric follow-up for another year to confirm that there was no further re-brightening. Throughout the event, the All-Sky Automated Survey for SuperNovae (ASAS-SN; Shappee et al. 2014; Kochanek et al. 2017) observed Gaia16aye serendipitously with a typical cadence of between two and five days. Its data cover various parts of the light curve of the event, including the part before the *Gaia* alert, where a smooth rise and the first caustic entry occurred.

2.1. Ground-based photometry calibrations

Each observatory processed the raw data with their own standard data reduction procedures to create bias, dark-subtracted, and flat-fielded images. Then, the images were solved astrometrically, most often with the use of `Astrometry.net` code (Hogg et al. 2008; Lang et al. 2010), and the instrumental photometry for all objects within the field of view was derived with a variety of tools, including Source EXtractor (Bertin & Arnouts 1996) and Daophot (Stetson 1987). The lists of detected sources with their measured instrumental magnitudes were uploaded to the Cambridge Photometric Calibration Server (CPCS)[3], designed and maintained by Sergey Koposov and Lukasz Wyrzykowski. The CPCS matches the field stars to a reference catalogue, identifies the target source, and determines which filter was used for observations. This tool acted as a central repository for all the data, but primarily, it standardised the data into a homogenous photometric system. It relied on available archival catalogues of this patch of the sky (primarily the AAVSO Photometric All-Sky Survey, APASS, and the Pan-STARRS1 Surveys, PS1) and derived zero-points for each of the observations. The use of a common repository allowed for near-real-time tracking of the evolution of the event, which is particularly important near the caustic entry and exit. Photometric data were uploaded by the observers within minutes of the

[2] https://www.astro-opticon.org/h2020/network/na4.html

[3] http://gsaweb.ast.cam.ac.uk/followup

Table 1. Telescopes used in the photometric follow-up observations of Gaia16aye.

Telescope code	Telescope/observatory name	Location	Longitude [deg]	Latitude [deg]	Reference
AAVSO	American Association of Variable Star Observers	world-wide network, MA, USA	–	–	–
Akeno50	50-cm telescope, Akeno Observatory	Asao, Akeno-mura, Japan	138.30	35.47	–
APT2	Automatic Photometric Telescope 2, Catania Astrophysical Observatory	Serra La Nave, Mt. Etna, Italy	14.97	37.69	–
Aries130	1.30-m telescope, Aryabhatta Research Institute of Observational Sciences	Manora Peak, Nainital, India	79.45	29.37	–
Aristarchos	Aristarchos Telescope, Helmos Observatory	Mt. Helmos, Peloponnese	22.20	37.99	Goudis et al. (2010)
ASASSN	All-Sky Automated Survey for Supernovae	world-wide network of 20 telescopes	–	–	Kochanek et al. (2017)
ASV1	Astronomical Station Vidojevica 0.6 m	Vidojevica, near Prokuplje, Serbia	21.56	43.14	–
ASV2	Astronomical Station Vidojevica 1.4 m	Vidojevica, near Prokuplje, Serbia	21.56	43.14	–
AUT25	25-cm telescope, Akdeniz University	Antalya, Turkey	30.66	36.90	–
BAS2	Rozhen 2 m, National Astronomical Observatory, Bulgarian Academy of Sciences	Rozhen, Bulgaria	24.74	41.70	–
BAS50/70	Schmidt-camera 50/70 cm, National Astronomical Observatory, Bulgarian Academy of Sciences	Rozhen, Bulgaria	24.74	41.70	–
Bialkow	Białków Observatory, Astronomical Institute of the University of Wrocław	Białków, Poland	16.66	51.48	–
C2PU	C2PU-Omicron, Center for Pedagogy in Planet and Universe sciences	OCA, Calern Plateau, France	6.92	43.75	–
Conti	Conti Private Observatory	MD, USA	−76.49	38.93	–
CrAO	Crimean Astrophysical Observatory	Nauchnyi, Crimea	34.01	44.73	–
DEMONEXT	DEdicated MONitor of EXotransits and Transients, Winer Observatory	AZ, USA	−110.60	31.67	Villanueva et al. (2018)
Foligno	Foligno Observatory	Perugia Province, Italy	12.70	42.96	–
HAO50	Horten Astronomical Telescope	Nykirke, Horten, Norway	10.39	59.43	–
Krakow50	50-cm Cassegrain telescope, Astronomical Observatory of Jagiellonian University	Kraków, Poland	19.82	50.05	–
Kryoneri	1.2-m Kryoneri telescope, Kryoneri Observatory	Mt. Kyllini, Peloponnese, Greece	22.63	38.07	Xilouris et al. (2018)
LCO-Texas	Las Cumbres Observatory	McDonald Observatory, TX, USA	−104.02	30.67	Brown et al. (2013)
LCO-Hawaii	Las Cumbres Observatory	Haleakala, HI, USA	−156.26	20.71	Brown et al. (2013)
Leicester	University of Leicester Observatory	Oadby, UK	−1.07	52.61	–
Loiano	1.52 m Cassini Telescope, INAF – Bologna Observatory of Astrophysics and Space Science	INAF-Bologna, Loiano, Italy	11.33	44.26	–
LOT1m	Lulin One-meter Telescope	Lulin Observatory, Taiwan	120.87	23.47	–
LT	Liverpool Telescope, Roque de Los Muchachos Observatory	La Palma, Spain	−17.88	28.76	Steele et al. (2004)
MAO165	1.65-m Ritchey-Chretien telescope, Molėtai Astronomical Observatory	Molėtai, Kulionys, Lithuania	25.56	55.32	–
Mercator	*Mercator* Telescope, Roque de Los Muchachos Observatory	La Palma, Spain	–17.88	28.76	–
Montarrenti	Montarrenti Observatory	Siena, Italy	11.18	43.23	–
OHP	T120, L'Observatoire de Haute-Provence	St. Michel, France	5.71	43.93	–
OndrejovD50	D50 telescope, Astronomical Institute of Academy of Sciences of the Czech Republic	Ondrejov, Czech Rep.	14.78	49.91	–
Ostrowik	Cassegrain telescope, Warsaw University Astronomical Observatory	Ostrowik, Poland	21.42	52.09	–
PIRATE	Physics Innovations Robotic Astronomical Telescope Explorer Mark-III, Teide Observatory	Tenerife, Spain	−16.51	28.30	– Kolb et al. (2018)
pt5m	0.5m robotic telescope, Roque de Los Muchachos Observatory	La Palma, Spain	−17.88	28.76	Hardy et al. (2015)
RTT150	1.5-m Russian-Turkish Telescope, TUBITAK National Observatory	Mt. Bakirlitepe, Antalya, Turkey	30.33	36.83	–
SAI	60-cm Zeiss-2 telescope, Moscow State Univercity	Nauchnyi, Crimea	34.01	44.73	–

Table 1. continued.

Telescope code	Telescope/observatory name	Location	Longitude [deg]	Latitude [deg]	Reference
	observational station of Sternberg Astronomical Institute				
Salerno	Salerno University Observatory	Fisciano, Italy	14.79	40.78	–
SKAS-KFU28	C28 CGEM-1100 telescope, Zelenchukskaya Station of Kazan Federal University	Zelenchukskaya, Caucasus, Russia	41.43	43.65	–
Skinakas	1.3-m telescope, Skinakas Observatory	Skinakas, Crete, Greece	24.90	35.21	–
SKYNET	Skynet Robotic Telescope Network, 41-inch telescope, Yerkes Observatory	WI, USA	−88.56	42.57	–
Swarthmore24	24-inch telescope, Peter van de Kamp Observatory	Swarthmore College, PA, USA	−75.36	39.91	–
T60	60-cm telescope, TUBITAK National Observatory	Mt. Bakirlitepe, Antalya, Turkey	30.33	36.83	–
T100	1.0-m telescope, TUBITAK National Observatory	Mt. Bakirlitepe, Antalya, Turkey	30.33	36.83	–
TJO	*Joan Oró* Telescope, Montsec Observatory	Sant Esteve de la Sarga, Lleida, Spain	0.73	42.03	–
TRT-GAO	Thai Robotic Telescope GAO, Yunnan Observatory	Phoenix Mountain, Kunming, China	105.03	26.70	–
TRT-TNO	Thai Robotic Telescope TNO, Thai National Observatory	Doi Inthanon, Chiang Mai, Thailand	98.48	18.57	–
UCLO-C14E	University College London Observatory, C14 East	Mill Hill, London, UK	−0.24	51.61	–
UCLO-C14W	University College London Observatory, C14 West	Mill Hill, London, UK	−0.24	51.61	–
UBT60	Akdeniz University Telescope, TUBITAK National Observatory	Mt. Bakirlitepe, Antalya, Turkey	30.33	36.83	–
Watcher	40-cm telescope, Boyden Observatory	Orange Free State, South Africa	26.40	–29.04	French et al. (2004)
WHT-ACAM	*William Herschel* Telescope, Roque de Los Muchachos Observatory	La Palma, Spain	−17.88	28.76	–
Wise1m	1.0-m telescope, Wise Observatory	Mitzpe Ramon, Israel	34.76	30.60	–
WiseC28	C28 Jay Baum Rich telescope, Wise Observatory	Mitzpe Ramon, Israel	34.76	30.60	–

observation, which facilitated detailed planning of the spectroscopic follow-up.

The list of all the ground-based photometric observations is summarised in Table 2 and the photometric observations are listed in Table C.1. The full table contains 23 730 entries and is available at the CDS. Figure 2 shows all follow-up measurements collected for Gaia16aye over a period of about one and a half years.

2.2. Gaia data

Since October 2014 *Gaia* collected 27 observations before the alert on the 5 August 2016. In total, *Gaia* observed Gaia16aye 84 times as of November 2018. The *G*-band photometric data points collected by *Gaia* are listed in Table B.1. Photometric uncertainties are not provided for *Gaia* alerts, and for this event we assumed 0.01 mag (Gaia Collaboration 2016), but as we show below, these were scaled to about 0.015 mag by requiring the microlensing model χ^2 per degree of freedom to be 1.0. Details of the *Gaia* photometric system and its calibrations can be found in Evans et al. (2018).

The on-board Radial Velocity Spectrometer (RVS) of *Gaia*, collects medium-resolution ($R \sim 11\,700$) spectra over the wavelength range 845–872 nm centred on the Calcium II triplet region of objects brighter than $V \sim 17$ mag (Gaia Collaboration 2016; Cropper et al. 2018). However, individual spectra for selected observations are made available already for brighter *Gaia* alerts using parts of the RVS data processing pipeline (Sartoretti et al. 2018). For Gaia16aye the RVS collected a spectrum on 21 November 2016, 17:05:47 UT (HJD = 2457714.21), see Fig. 3, the moment is caught by *Gaia* at very high magnification, when Gaia16aye reached $G = 12.91$ mag. The exposure time for the combined three RVS CCDs was 3×4.4 s.

2.3. Spectroscopy

Spectroscopic measurements of the event were obtained at various stages of its evolution. The list of spectroscopic observations is presented in Table 3. The very first set of spectra was taken with the Asiago 1.22 m telescope equipped with the DU440A-BU2 instrument, the Asiago 1.82 m telescope with AFOSC, and the SPRAT instrument on the 2 m Liverpool Telescope (LT), which showed no obvious features seen in outbursting Galactic variables. Other spectra gathered by the 5 m P200 Palomar Hale Telescope and by ACAM on the 4.2 m WHT confirmed this behaviour. This therefore led us to conclude that this is a microlensing event.

We did not find significant differences between spectra taken at various consecutive stages of the event evolution. The features and general shape of the spectra were the same, regardless of whether the spectrum was recorded during amplification or in the baseline. This allows us to conclude that the spectra were dominated by radiation from the source, and contribution from the lens was negligible.

Most of the spectra were obtained in low-resolution mode ($R \leq 1000$) and relatively poor weather conditions, which were useful for an early classification of the transient as a microlensing event. A more detailed analysis of the low-resolution spectra will be presented elsewhere (Zielinski et al., in prep.).

Table 2. Summary of observations taken by the observatories involved in the photometric follow-up of Gaia16aye.

Telescope code	First epoch [HJD-2450000]	Last epoch [HJD-2450000]	Npoints (filter), Npoints (filter2), etc.
AAVSO	7653.283	7714.561	288(V) 151(i) 95(r)
Akeno50	7711.012	7715.301	169(r)*
APT2	7612.294	8055.256	285(B) 467(V) 439(i) 452(r)
Aries130	7714.070	7718.030	6(B) 6(V) 6(R) 6(I)
Aristarchos	8035.219	8039.086	2(B) 2(V) 1(g) 6(i) 44(r)
ASASSN	7547.097	7907.897	68(V)*
ASV1	7929.570	8079.302	11(B) 34(V) 36(i) 28(r)
ASV2	7628.483	7924.511	42(B) 64(V) 1(g) 69(i) 73(r)
AUT25	7712.258	7715.274	136(i) 142(r)
BAS2+BAS50/70	7687.225	7933.497	8(B) 23(V) 9(g) 28(i) 31(r)
Bialkow	7619.340	8028.296	218(B) 499(V) 657(i) 641(r)
C2PU	7637.331	7878.619	8(V) 41(r)
Conti	7714.470	7714.510	38(V)
CrAO	7710.306	7871.562	639(r)
DEMONEXT	7690.672	8162.029	476(V) 483(i) 427(r)
Foligno	7654.361	7719.251	11(V)
HAO50	7818.318	8056.320	22(V)*, 10(R)*
Krakow50	7659.243	7919.552	17(B) 44(V) 49(i) 60(r)
Kryoneri	7652.327	8039.210	92(i) 96(r)
LCO-Texas	7663.570	7904.530	63(B) 70(V) 30(g) 29(i) 94(r)
LCO-Hawaii	6792.778	7708.778	197(gp)*, 318(rp)*, 518(ip)*, 294(V)*, 146(B)*, 24(R)*, 12(I)*
Leicester	7645.461	8063.274	10(B) 9(V) 3(i) 1(r)
Loiano	7660.301	7709.269	77(B) 66(V) 108(g) 119(i) 164(r)
LOT1m	7711.936	7888.223	54(g) 59(i) 55(r)
LT	7647.327	7976.490	2(V) 362(g) 415(i) 488(r)
MAO165	7680.350	7997.400	6(B)* 31(V)* 34(R)* 27(I)*
Mercator	7651.332	7657.397	7(g) 5(r)
Montarrenti	7654.280	7929.545	92(r)
OHP	7665.329	8019.350	6(V) 3(g) 11(i) 13(r)
OndrejovD50	7614.564	8095.253	397(B) 410(V) 413(i) 423(r)
Ostrowik	7619.303	7735.192	3(B) 42(V) 1(g) 185(i) 193(r)
PIRATE	7650.498	7849.748	1473(r) 713(V)
pt5m	7610.408	8094.350	205(B) 2452(V) 243(i) 266(r)
RTT150	7657.696	7937.559	114(B) 112(V) 1(g) 1(i) 1(r)
SAI	7610.282	7613.265	16(B) 16(V) 18(r)
Salerno	7651.308	7765.244	610(R)*
SKAS-KFU28	7662.357	7846.548	124(B)* 158(G)* 170(R)*
Skinakas	7668.246	7993.770	5(B) 1(G) 5(V) 2(g) 6(i) 5(r)
SKYNET	7670.521	7729.487	6(g) 64(i) 38(r)
Swarthmore24	7714.444	7954.598	287(i)
T60	7670.862	8436.268	1(B) 9(V) 8(r) 8(i)
T100	7637.476	7963.499	27(B) 34(V) 24(g) 21(i) 21(r)
TJO	7610.503	8090.273	485(B) 563(V) 1(g) 494(i) 524(r) 2(z)
TRT-GAO	7712.986	7886.388	3(V) 1016(r)
TRT-TNO	7833.368	7843.437	41(i) 48(r)
UCLO-C14E	7678.287	7711.319	5(V) 28(r)
UCLO-C14W	7666.399	7955.577	122(i) 44(r)
UBT60	7610.246	7715.274	279(B) 349(V) 440(i) 448(r)
Watcher	7617.004	8017.002	258(V) 264(i) 261(r)
WHT-ACAM	7701.314	7701.375	26(g) 30(i) 30(r)
Wise1m	7654.236	7749.173	305(i)
WiseC28	7652.396	7660.294	25(i)

Notes. In brackets we list the best-matching filters as found by the Calibration Server. Asterisks mark data that were not uploaded to the CPCS.

We also obtained spectra of higher resolution ($R \sim 6500$) with the 2.5 m INT, La Palma, Canary Islands, during three consecutive nights on 19−21 November 2016. The INT spectra were obtained using the Intermediate Dispersion Spectrograph (IDS, Cassegrain Focal Station, 235 mm focal length camera RED+2) with the grating set to R1200Y, and a dispersion of 0.53 Å pixel^{-1} with a slit width projected onto the sky equal to 1.298″ (see Table 3, spectrum INT 3–5). The exposure time was 400 s for each spectrum centred at wavelength 8100 Å.

The spectra were processed by the observers with their own pipelines or in a standard way using IRAF[4] tasks and scripts. The reduction procedure consisted of the usual bias- and dark-subtraction, flat-field correction, and wavelength calibration.

[4] IRAF is distributed by the National Optical Astronomy Observatories, which are operated by the Association of Universities for Research in Astronomy, Inc., under cooperative agreement with the National Science Foundation.

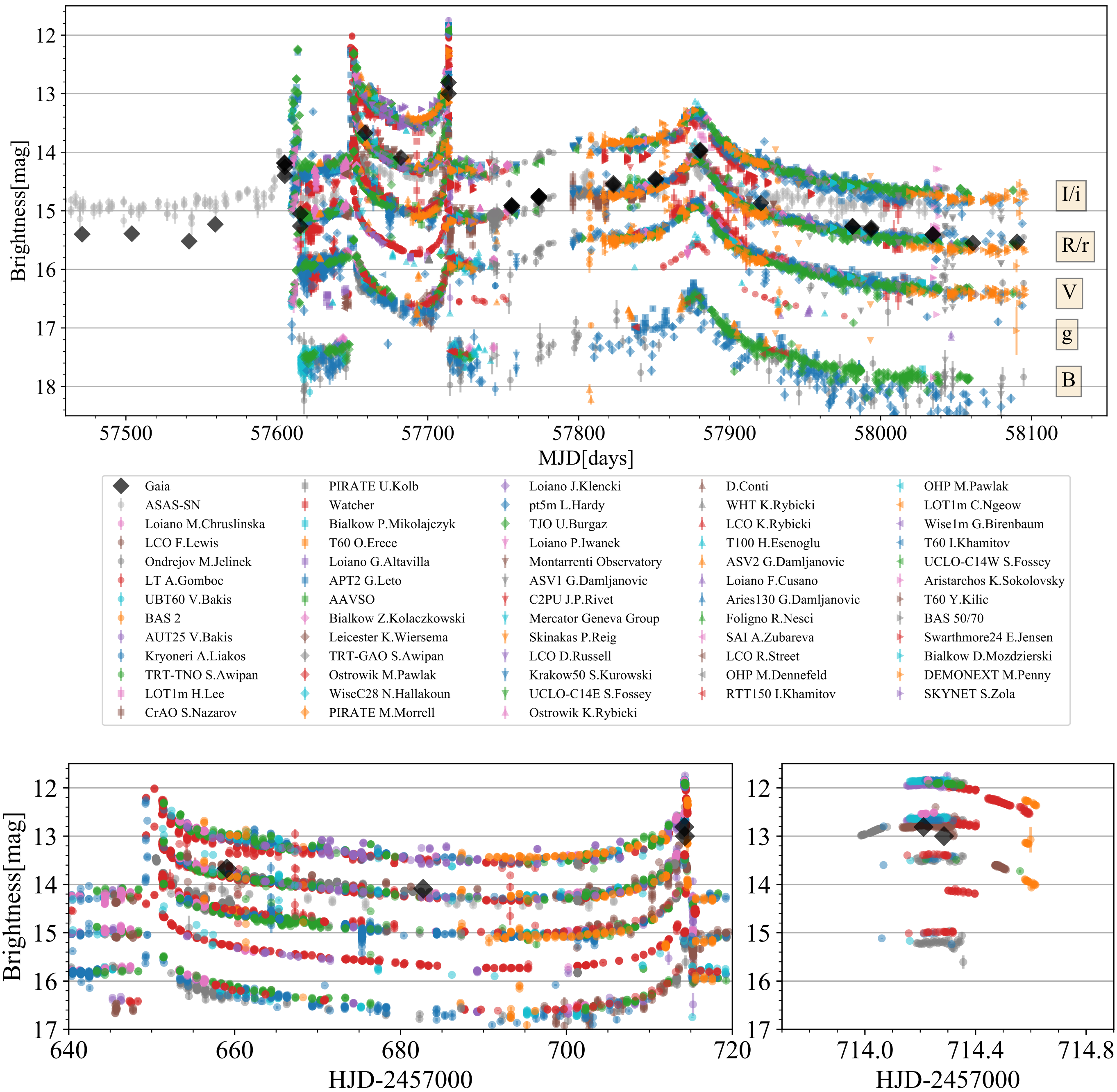

Fig. 2. *Gaia*, ASAS-SN, and follow-up photometric observations of Gaia16aye. Each observatory and observer is marked with a different colour. The marker is explained in the legend. The figure shows only the follow-up data, which were automatically calibrated using the Cambridge Photometric Calibration Server. *Upper panel*: entire event, and *bottom panels*: zoom on the second pair of caustic crossings (*left*) and a detail of the fourth caustic crossing (*right*).

2.4. Swift observations

In order to rule out the possibility that Gaia16aye is some type of cataclysmic variable star outburst, we requested X-ray and ultraviolet *Swift* observations. *Swift* observed Gaia16aye for 1.5 ks on 18 August 2016. *Swift*/XRT detected no X-ray source at the position of the transient with an upper limit of 0.0007 ± 0.0007 cts s^{-1} (a single background photon appeared in the source region during the exposure). Assuming a power-law emission with a photon index of 2 and HI column density of 43.10×10^{20} cm^{-2} (corresponding to the total Galactic column density in this direction; Kalberla et al. 2005), this translates into an unabsorbed 0.3–10 keV flux limit of 5.4×10^{-14} ergs cm^{-2} s^{-1}.

No ultraviolet source was detected by the UVOT instrument at the position of the transient. The upper limit at epoch HJD′ = 7618.86 was derived as >20.28 mag for UVM2-band (Vega system).

2.5. Keck adaptive optics imaging

The event was observed with Keck adaptive optics (AO) imaging on 8 October 2016 (HJD′ = 7669.7). Figure 4 shows the

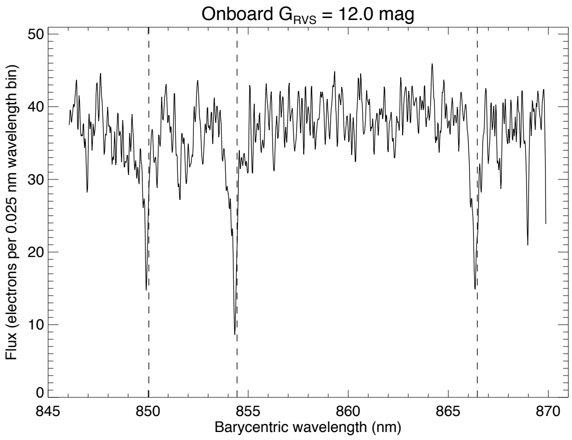

Fig. 3. Medium-resolution spectrum of the Gaia16aye event obtained with the *Gaia* RVS at the brightest moment of the event as seen by *Gaia* at the fourth caustic crossing. The Ca II lines of the lensed source are clearly visible.

10 arcsec field of view obtained with the Keck AO instrument. The full width at half-maximum (FWHM) of the star is about 52 mas. The image shows a single object with no additional light sources in its neighbourhood. This indicates that no additional luminous components contributed to the observed light.

3. Spectroscopy of the source star

During a microlensing event, the variation in the amplification changes the ratio of the flux from the source, while the blend or lens light remains at the same level. Therefore, the spectroscopic data obtained at different amplifications can be used to de-blend the light of the source from any additional constant components and to derive the source properties.

In order to obtain the spectral type and stellar parameters of the Gaia16aye source, we used three spectra gathered by the 2.5 m INT. Based on these spectra we were able to determine the atmospheric parameters of the microlensing source. We used a dedicated spectral analysis framework, iSpec[5], which integrates several radiative transfer codes (Blanco-Cuaresma et al. 2014). In our case, the SPECTRUM code was used (Gray & Corbally 1994), together with well-known Kurucz model atmospheres (Kurucz 1993) and solar abundances of chemical elements taken from Asplund et al. (2009). The list of absorption lines with atomic data was taken from the VALD database (Kupka & Dubernet 2011). We modelled synthetic spectra for the whole wavelength region between 7200 and 8800 Å. The spectrum that was synthesized to the observational data with the lowest χ^2 value constituted the final fit generated for specific atmospheric parameters: effective temperature ($T_{\rm eff}$), surface gravity (log g), and metallicity ([M/H]). For simplification purposes, we adopted solar values of micro– and macroturbulence velocities and also neglected stellar rotation. The resolution of the synthetic spectra was fixed as $R = 10\,000$. We applied this method to all three INT spectra independently and then averaged the results. The mean values for the source parameter in Gaia16aye were as follows: $T_{\rm eff} = 3933 \pm 135$ K, log $g = 2.20 \pm 1.44$, and [M/H] = 0.08 ± 0.41 dex. Figure 5 presents the best fit of the synthetic to observational INT spectrum in the same spectral region as was covered by the RVS spectrum of Gaia16aye, that is, 8400–8800 Å (Ca II triplet), generated for averaged parameter results. These parameters imply that the microlensing source is a K5-type giant or a super-giant with solar metallicity. We discuss the estimate for the source distance in the next section because it is first necessary to de-blend the light of the lens and the source, which is possible in the microlensing model. We note that the asymmetry of the *Gaia* RVS lines is not visible in the same-resolution INT/IDS spectrum, and we suspect that the broadening visible in the *Gaia* spectrum is a result of a stack of spectra from separate RVS CCDs.

[5] https://www.blancocuaresma.com/s/iSpec

4. Microlensing model

4.1. Data preparation

The data sets we used in the modelling are listed in Table D.1. Because the microlensing model is complex, we had to restrict the number of data points that were used. We chose data sets that cover large parts of the light curve or important features (such as caustics). Some of the available data sets were also disregarded because they showed strong systematic variations in residuals from the best-fit model, which are not supported by other data sets. We used observations collected in the Cousins I or Sloan i band because the signal-to-noise ratio in these filters is highest. The only exceptions were *Gaia* (G-band filter) and ASAS-SN data (V band), which cover large portions of the light curve, especially before the transient alert.

Calculating microlensing magnifications (especially during caustic crossings) requires much computational time. We thus binned the data to speed up the modelling. We commonly used one-day bins, except for caustic crossings (when brightness variations during one night are substantial), for which we used 0.5 h or 1 h bins. *Gaia* and ASAS-SN data were not binned.

We rescaled the error bars, so that χ^2/d.o.f. ~ 1 for each data set. The error bars were corrected using the formula $\sigma_{i,\rm new} = \sqrt{(\gamma\sigma_i)^2 + \epsilon^2}$. Coefficients γ and ϵ for each data set are shown in Table 4. The final light curve is presented in Fig. 6.

4.2. Binary lens model

The simplest model describing a microlensing event caused by a binary system needs seven parameters: the time of the closest approach between the source and the centre of mass of the lens t_0, the projected separation between source and barycenter of the lens at that time u_0 (in Einstein radius units), the Einstein crossing time $t_{\rm E}$, the mass ratio of the lens components q, the projected separation between two binary components s, the angle between the source–lens relative trajectory and the binary axis α, and the angular radius of the source ρ normalised to the Einstein radius (Eq. (1)).

This simple model is insufficient to explain all features in the light curve. We therefore included additional parameters that describe second-order effects: the orbital motion of the Earth (microlensing parallax) and the orbital motion of the lens. The microlensing parallax $\boldsymbol{\pi}_{\rm E} = (\pi_{\rm E,N}, \pi_{\rm E,E})$ is a vector quantity: $\boldsymbol{\pi}_{\rm E} = \frac{\pi_{\rm rel}}{\theta_{\rm E}} \frac{\boldsymbol{\mu}_{\rm rel}}{\mu_{\rm rel}}$, where $\boldsymbol{\mu}_{\rm rel}$ is the relative lens-source proper motion (Gould 2000). It describes the shape of the relative lens-source trajectory (Fig. 7). The microlensing parallax can also be measured using simultaneous observations from two separated observatories, for exmaple, from the ground and a distant satellite (Refsdal 1966; Gould 1994). Because *Gaia* is located at the L_2 Lagrange point (about 0.01 au from the Earth) and the Einstein radius projected onto the observer's plane is au/$\pi_{\rm E} \approx 2.5$ au, the magnification gradient changes by less than the data precision throughout most of the light curve (see

Table 3. Summary of the spectroscopic observations of Gaia16aye.

Spectrum ID	Observation date HJD	Wavelength range (Å)	Telescope – Instrument
LT 1	2457612.900668	4200–7994	Liverpool Telescope – SPRAT
LT 2	2457617.940097	4200–7994	Liverpool Telescope – SPRAT
LT 3	2457643.845837	4200–7994	Liverpool Telescope – SPRAT
WHT 1	2457701.3045827	4303–9500	*William Herschel* Telescope – ACAM
Palomar 1	2457662.1047682	3100–10200	Palomar Hale Telescope – DBSP
Palomar 2	2457932.6881373	3800–10000	Palomar Hale Telescope – DBSP
INT 1	2457703.4230518	7550–9000	*Isaac Newton* Telescope – IDS; R831R grating
INT 2	2457706.3547417	7550–9000	*Isaac Newton* Telescope – IDS; R831R grating
INT 3	2457712.2970278	7500–8795	*Isaac Newton* Telescope – IDS; R1200Y grating
INT 4	2457713.2967616	7500–8795	*Isaac Newton* Telescope – IDS; R1200Y grating
INT 5	2457714.2949097	7500–8795	*Isaac Newton* Telescope – IDS; R1200Y grating
Asiago 1	2457612.430953	3320–7880	1.22 m Reflector – DU440A-BU2
Asiago 2	2457623.364186	4160–6530	1.82 m Reflector – AFOSC; GR07 grating
Asiago 3a	2457700.264730	8200–9210	1.82 m Reflector – AFOSC; VPH5 grating
Asiago 3b	2457700.275567	5000–9280	1.82 m Reflector – AFOSC; VPH6 grating
Asiago 4a	2457700.260113	8200–9210	1.82 m Reflector – AFOSC; VPH5 grating
Asiago 4b	2457700.270951	5000–9280	1.82 m Reflector – AFOSC; VPH6 grating
Asiago 5a	2457722.263836	8200–9210	1.82 m Reflector – AFOSC; VPH5 grating
Asiago 5b	2457722.235417	5000–9280	1.82 m Reflector – AFOSC; VPH6 grating
Asiago 6a	2457723.246689	8200–9210	1.82 m Reflector – AFOSC; VPH5 grating
Asiago 6b	2457723.204078	5000–9280	1.82 m Reflector – AFOSC; VPH6 grating

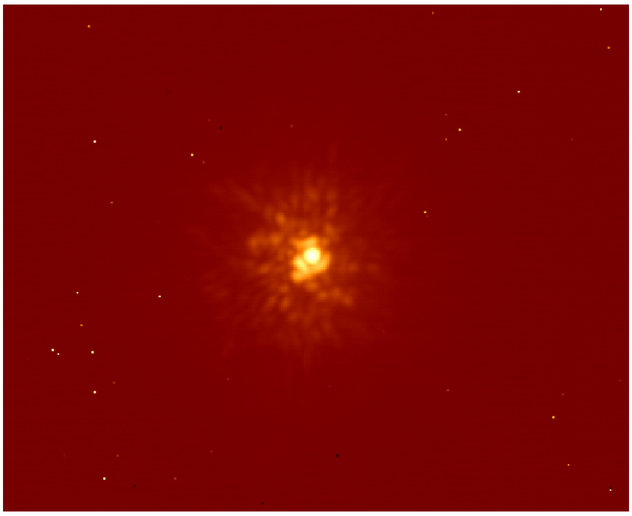

Fig. 4. Keck Adaptive Optics image of Gaia16aye taken between the third and fourth caustic crossing. The single star has an FWHM of about 52 mas. No other light sources contribute significantly to the blending in the event.

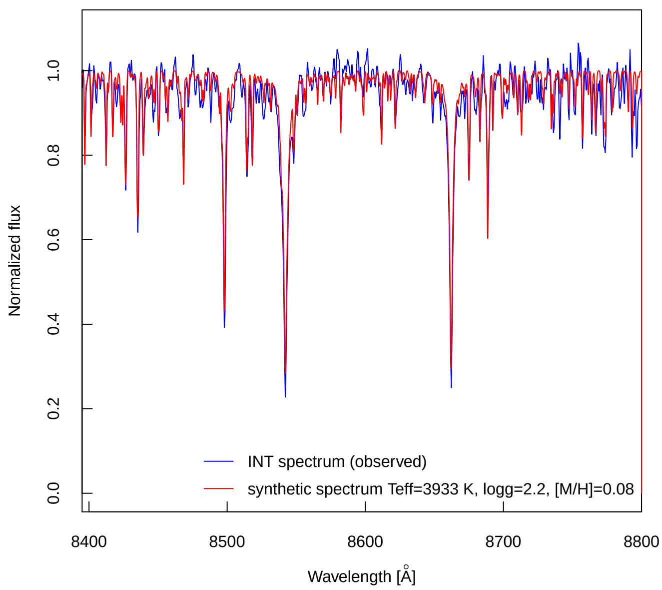

Fig. 5. Spectrum of the source of the Gaia16aye event (blue) taken using the 2.5 m INT/IDS on 19 November 2016 in comparison with a synthetic spectrum (red) calculated for the best-fit atmospheric parameters. The plot shows the Ca II triplet region, 8400–8800 Å.

Fig. 8). Fortunately, two *Gaia* measurements were collected near HJD′ ∼ 7714, when the space-parallax signal is strongest due to rapid change in magnification near the caustic. Therefore, we included the space-parallax and *Gaia* observations in the final modelling.

The orbital motion of the lens can in the simplest scenario be approximated as linear changes of separation $s(t) = s_0 + \dot{s}(t - t_{0,\rm kep})$ and angle $\alpha(t) = \alpha_0 + \dot{\alpha}(t - t_{0,\rm kep})$, $t_{0,\rm kep}$ can be any arbitrary moment of time and is not a fit parameter (Albrow et al. 2000). This approximation, which works well for the majority of binary microlensing events, is insufficient in this case.

We have to describe the orbital motion of the lens using a full Keplerian approach (Skowron et al. 2011). This model is parameterised by the physical relative 3D position and velocity of the secondary component relative to the primary, $\Delta \boldsymbol{r} = D_{\rm l}\theta_{\rm E}(s_0, 0, s_z)$, $\Delta \boldsymbol{v} = D_{\rm l}\theta_{\rm E} s_0(\gamma_x, \gamma_y, \gamma_z)$ at time $t_{0,\rm kep}$. For a given angular radius of the source star θ_* and source distance $D_{\rm s}$, we can calculate the angular Einstein radius $\theta_{\rm E} = \theta_*/\rho$ and distance to the lens $D_{\rm l} = {\rm au}/(\theta_{\rm E}\pi_{\rm E} + {\rm au}/D_{\rm s})$. Subsequently, positions and

Table 4. Data sets used in the modelling.

Observatory	Filter	Number	γ	ϵ
Gaia	G	53	1.4	0.0
Bialkow	I	72	1.15	0.005
APT2	I	156	1.70	0.01
LT	i	94	1.15	0.005
DEMONEXT	I	110	1.35	0.005
Swarthmore	I	19	1.00	0.00
UBT60	I	18	1.00	0.005
ASAS-SN	V	68	1.45	0.01

velocities can be transformed to orbital elements of the binary (semi-major axis a, orbital period P, eccentricity e, inclination i, longitude of the ascending node Ω, argument of periapsis ω, and time of periastron $t_{\rm peri}$). These can be used to calculate the projected position of both components on the sky at any moment in time.

In all previous cases of binary events with significant binary motion, Keplerian orbital motion provided only a small improvement relative to the linear approximation (Skowron et al. 2011; Shin et al. 2012). This is not the case here, because, as we show below, the orbital period of the lens is similar to the duration of the event (e.g. Penny et al. 2011). Modelling of this event is an iterative process: for given microlensing parameters, we estimated the angular radius and distance to the source, we calculated best-fit microlensing parameters, and we repeated the procedure until all parameters converged.

The best-fit microlensing parameters are presented in Table 5. Uncertainties were calculated using the Markov chain Monte Carlo approach (MCMC; Foreman-Mackey et al. 2013) and represent 68% confidence intervals of marginalized posterior distributions. We note that another degenerate solution exists for the microlensing model that differs only by the signs of s_z and γ_z ($(s_z, \gamma_z) \rightarrow -(s_z, \gamma_z)$). The second solution has the same physical parameters (except for $\Omega \rightarrow \pi - \Omega$ and $\omega \rightarrow \omega - \pi$) and differs by the sign of the radial velocity. Thus, the degeneracy can be broken with additional radial velocity measurements of the lens (Skowron et al. 2011).

4.3. Source star

Spectroscopic observations of the event indicate that the source is a K5-type giant or a super-giant. If the effective temperature of the source were higher than 4250 K, TiO absorption features would be invisible. If the temperature were lower than 3800 K, these features would be stronger than those in the observed spectra. Spectral modelling indicates that the effective temperature of the source is 3933 ± 135 K. According to Houdashelt et al. (2000), the intrinsic Johnson–Cousins colours of a star of this spectral type and solar metallicity should be $(V-R)_0 = 0.83^{+0.03}_{-0.12}$, $(V-I)_0 = 1.60^{+0.03}_{-0.12}$ and $(V-K)_0 = 3.64^{+0.11}_{-0.37}$ (error bars correspond to the source of K4- and M0-type, respectively).

We used a model-independent regression to calculate the observed colours of the source (we used observations collected in the Bialkow Observatory, which were calibrated to the standard system): $V-R = 0.99 \pm 0.01$ and $V-I = 1.91 \pm 0.01$. Thus, the colour excess is $E(V-I) = 0.31$ and $E(V-R) = 0.16$, consistent with the standard reddening law (Cardelli et al. 1989) and $A_V = 0.62$.

According to the best-fitting microlensing model, the amount of light coming from the magnified source is $V_{\rm s} = 16.61 \pm 0.02$ and $I_{\rm s} = 14.70 \pm 0.02$. The V-band brightness of the source after correcting for extinction is therefore $V_0 = 15.99$ mag. Subsequently, we used the colour–surface brightness relations for giants from Adams et al. (2018) to estimate the angular radius of the source: $\theta_* = 9.2 \pm 0.7\,\mu$as. Because the linear radius of giants of this spectral type is about $31 \pm 6\,R_\odot$ (Dyck et al. 1996), the source is located about 15.7±3.0 kpc from the Sun, but the uncertainties are large. For the modelling we assumed $D_{\rm s} = 15$ kpc. We note that the exact value of the distance has in practice a very small effect on the final models because $\pi_{\rm s} \ll \theta_{\rm E}\pi_{\rm E}$.

4.4. Physical parameters of the binary lens

The Gaia16aye microlensing model allows us to convert microlensing quantities into physical properties of the lensing binary system. Finite source effects over the caustics enabled us to measure the angular Einstein radius,

$$\theta_{\rm E} = \frac{\theta_*}{\rho} = 3.04 \pm 0.24\,{\rm mas}$$

and the relative lens-source proper motion,

$$\mu_{\rm rel} = \frac{\theta_{\rm E}}{t_{\rm E}} = 10.1 \pm 0.8\,{\rm mas\,yr^{-1}}.$$

Because the microlensing parallax was precisely measured from the light curve (Table 5), we were able to measure the total mass of the lens,

$$M = \frac{\theta_{\rm E}}{\kappa\pi_{\rm E}} = 0.93 \pm 0.09\,M_\odot$$

and its distance,

$$D_{\rm l} = \frac{\rm au}{\theta_{\rm E}\pi_{\rm E} + {\rm au}/D_{\rm s}} = 780 \pm 60\,{\rm pc}.$$

The orbital parameters of the lens were calculated using the prescriptions from Skowron et al. (2011) based on the full information about the relative 3D position and velocity of the secondary star relative to the primary. All physical parameters of the lens are given in Table 6. Figure 9 shows the orbital parameters and their confidence ranges as derived from the MCMC sampling of the microlensing model. Our microlensing model also allowed us to separate the flux from the source and the unmagnified blended flux (that comes from the lens, as we show below): $V_{\rm blend} = 17.98 \pm 0.02$, $R_{\rm blend} = 17.05 \pm 0.02$, and $I_{\rm blend} = 16.09 \pm 0.02$ (Table 5).

5. Discussion

A massive follow-up campaign allowed us to collect a very detailed light curve for *Gaia* 16aye and hence to cover the evolution of the event exhaustively. Photometric data were obtained over a period of more than two years by a network of observers scattered around the world. It should be emphasised that the vast majority of the observations were taken by enthusiastic individuals, including both professional astronomers and amateurs, who devoted their telescope time to this task.

The case of Gaia16aye illustrates the power of coordinated long-term time-domain observations, which lead to a scientific discovery. The field of microlensing has particularly well benefit in the past from such follow-up observations, which resulted, for example, in the first microlensing planetary discoveries (e.g. Udalski et al. 2005; Beaulieu et al. 2006). This event also

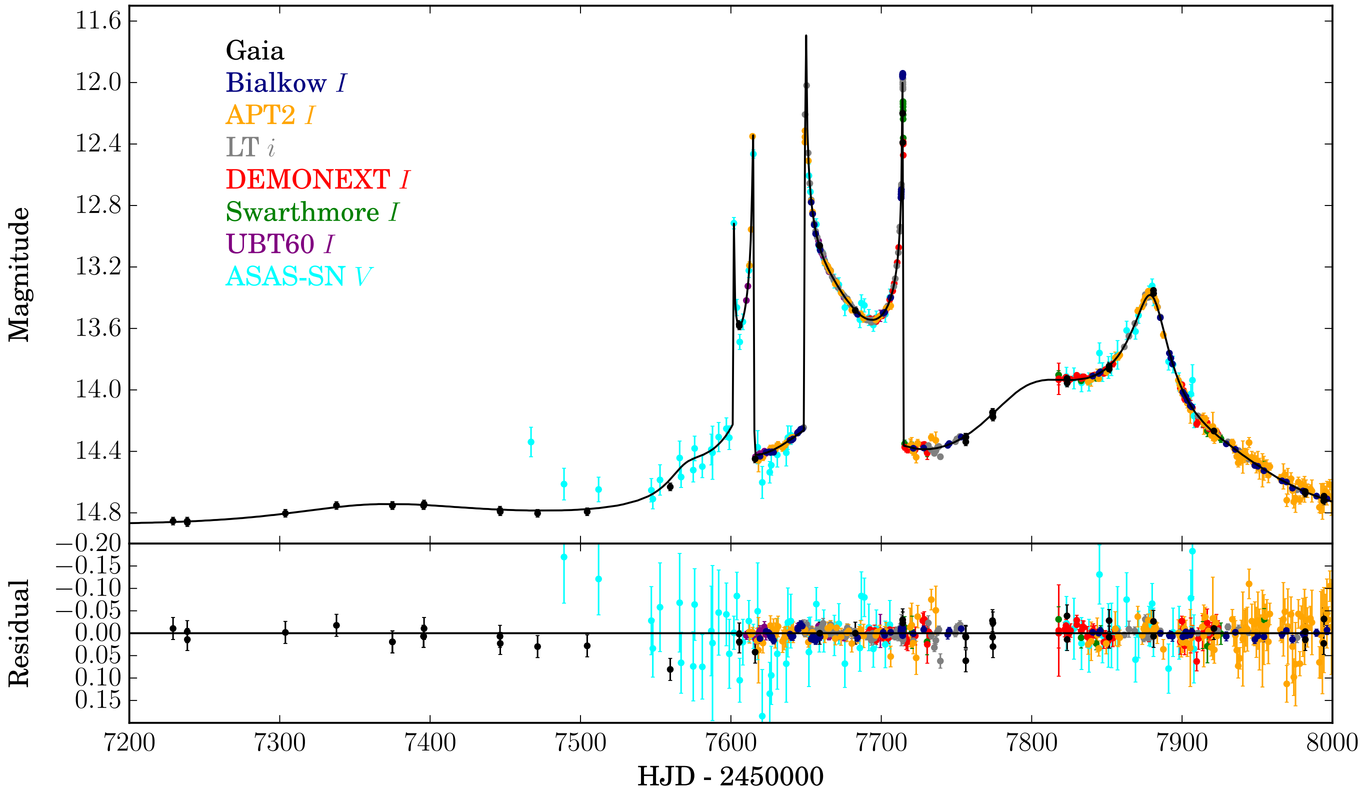

Fig. 6. Light curve of the microlensing event Gaia16aye, showing only the data used in the microlensing model. All measurements are transformed into the LT i-band magnitude scale.

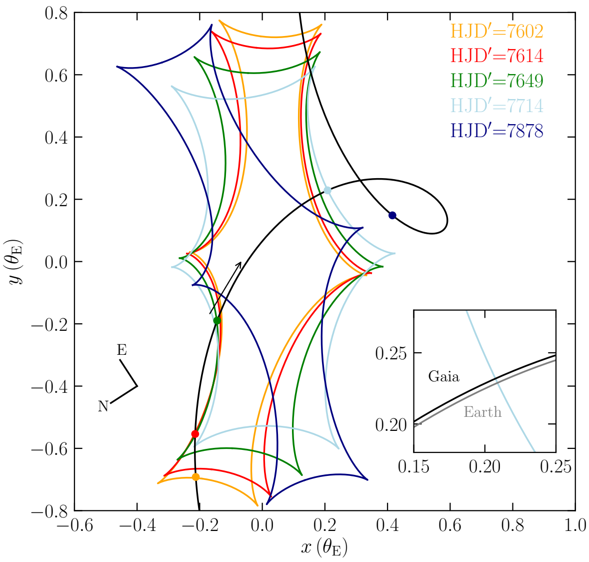

Fig. 7. Caustic curves corresponding to the best-fitting model of Gaia16aye. The lens-source relative trajectory is shown by a black curve. The barycenter of the lens is at (0, 0) and the lens components are located along the x-axis at time $t_{0,\mathrm{kep}} = 7675$. Caustics are plotted at the times of caustic crossings; the large points are marked with respective colours. The inset shows a zoom on the trajectory of the Earth and *Gaia* at the moment of the caustic crossing around HJD′ ∼ 7714.

offered excitement with its multiple, rapid, and often dramatic changes in brightness. Therefore it was also essential to use tools that facilitated the observations and data processing. Of particular importance was the Cambridge Photometric Calibration Server (CPCS, Zieliński et al. 2019), which performed the standardisation of the photometric observations collected by a large variety of different instruments. Moreover, the operation of the CPCS can be scripted, hence the observations could be automatically uploaded and processed without any human intervention. This solution helped track the evolution of the light curve, especially at times when the event changed dramatically. The processed observations and photometric measurements were immediately available for everyone to view, and appropriate actions were undertaken, such as an increase of the observing cadence when the peak at the fourth caustic crossing was approached. We note that no archival catalogues are available in I and R filters for the part of the sky with the Gaia16aye event. All the observations carried out in these filters were automatically adjusted by the CPCS to the nearest Sloan i and r bands. This does not affect the microlensing modelling, but the standardised light curve in i and r filters is systematically offset. On the other hand, the B-, g- and V-band observations processed by the CPCS are calibrated correctly to the 1% level.

In the case of Gaia16aye, the light curve contains multiple features, which allowed us to constrain the microlensing model uniquely, despite its complexity. In addition to the four caustic crossings and a cusp approach, the microlensing model also predicted a smooth low-amplitude long-term bump about a year before the first caustic crossing, at about HJD′ = 7350. This feature was indeed found in the *Gaia* data, see Fig. 6. The amplitude of this rise was about 0.1 mag, which is close to the level of *Gaia*'s photometric error bars, and the signal was far too faint to trigger an alert.

Additional confirmation of the correctness of the microlensing model comes from the detection of the microlensing space-parallax effect, see Fig. 8. The offset in the timing of the fourth

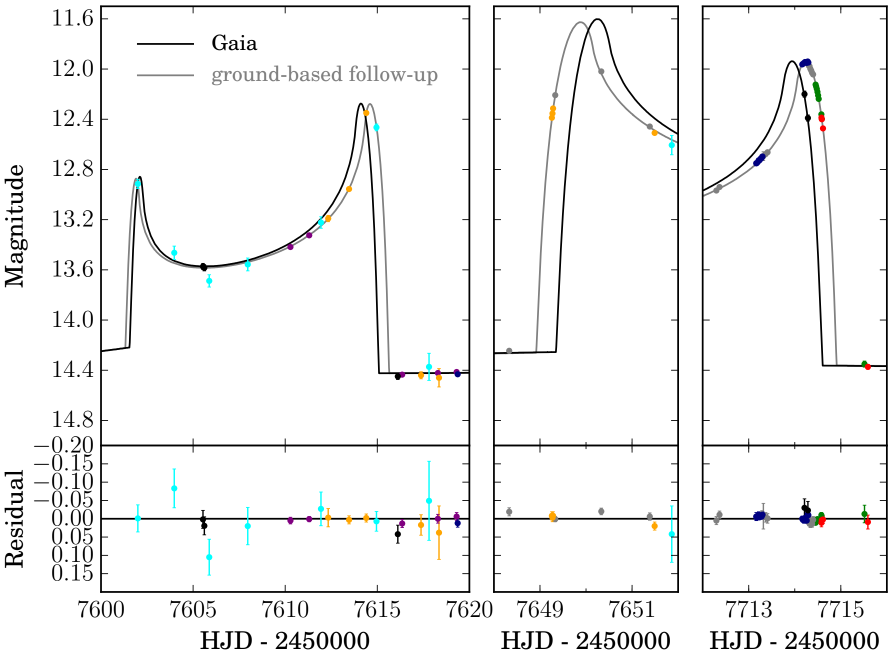

Fig. 8. Space-based parallax in Gaia16aye. As *Gaia* is separated by 0.01 au from the Earth, the *Gaia* light curve (black) differs slightly from Earth-based observations (grey curve). Space parallax can be measured through two fortuitous *Gaia* data points collected near HJD′ ~ 7714. All measurements are transformed into the LT *i*-band magnitude scale.

Table 5. Best-fit microlensing model parameters of the Gaia16aye binary event.

Parameter	Value
t_0 (HJD′)	7674.738 ± 0.057
u_0	0.0400 ± 0.0014
t_E (d)	111.09 ± 0.41
$\pi_{E,N}$	−0.373 ± 0.002
$\pi_{E,E}$	−0.145 ± 0.001
$\log\rho$	−2.519 ± 0.003
q	0.639 ± 0.004
s_0	1.007 ± 0.002
α (rad)	5.339 ± 0.002
s_z	0.404 ± 0.028
γ_x (yr^{-1})	0.384 ± 0.009
γ_y (yr^{-1})	0.591 ± 0.012
γ_z (yr^{-1})	−1.121 ± 0.032
I_s (mag)	14.70 ± 0.02
I_{blend} (mag)	16.09 ± 0.02
R_s (mag)	15.62 ± 0.02
R_{blend} (mag)	17.05 ± 0.02
V_s (mag)	16.61 ± 0.02
V_{blend} (mag)	17.98 ± 0.02

Notes. HJD′ = HJD-2450000. We adopt $t_{0,par} = t_{0,kep} = 7675$.

Table 6. Physical parameters of the binary lens system.

Parameter	Value
θ_E (mas)	3.04 ± 0.24
μ_{rel} (mas yr^{-1})	10.1 ± 0.8
M_1 ($M_\odot$)	0.57 ± 0.05
M_2 ($M_\odot$)	0.36 ± 0.03
D_l (pc)	780 ± 60
a (au)	1.98 ± 0.03
P (yr)	2.88 ± 0.05
e	0.30 ± 0.03
i (deg)	65.5 ± 0.7
Ω (deg)	−169.4 ± 0.9
ω (deg)	−30.5 ± 3.8
t_{peri} (HJD′)	8170 ± 14

Notes. Uncertainties of orbital parameters do not include the uncertainty in θ_* and D_s. We adopt $\theta_* = 9.2\,\mu$as and $D_s = 15$ kpc.

caustic crossing as seen by *Gaia* and ground-based telescopes is due to the distance of *Gaia* of 1.5 million km away from Earth. The offset in time was 6.63 h (i.e. the caustic crossing by the source occurred first at *Gaia*'s location) and the amplification difference was −0.007 mag, that is, it was brighter at *Gaia*. The model from ground-based data only predicted these offsets to within 3 min and 0.003 mag, respectively. This indicates our model is unique and robust.

From the microlensing light curve analysis, we can derive an upper limit on the amount of light emitted by the lensing object, or constraints on the dark nature of the lens can be obtained (e.g. Yee 2015; Wyrzykowski et al. 2016). We find that the masses of the lens components are 0.57 ± 0.05 $M_\odot$ and 0.36 ± 0.03 $M_\odot$ and that the lens is located about D_l = 780 ± 60 pc from the Sun. Because the V-band absolute magnitudes of main-sequence stars of these masses are 8.62 and 11.14 (Pecaut & Mamajek 2013), respectively, the total brightness of the binary is V = 17.97 and I = 16.26, assuming conservatively A_V = 0.1 towards the lens. This is consistent with the brightness and colour of the blend (V_{blend} = 17.98 and I_{blend} = 16.09). The blended light therefore comes from the lens, which is also consistent with the lack of any additional sources of light on the Keck AO image. This is an additional check that our model is correct.

The largest uncertainty in our lens mass determination comes from the θ_E parameter, which we derived from the finite source effects. Through the multiple caustic crossings, but particularly through very detailed coverage of the fourth crossing with multiple observatories, we were able to constrain the size of the source stellar disc in units of the Einstein radius ($\log\rho$) with an uncertainty smaller than 1%. However, in order to derive θ_E, we relied on the colour-angular size relation and theoretical predictions for the de-reddened colour of the source based on its spectral type. These may have introduced systematic errors

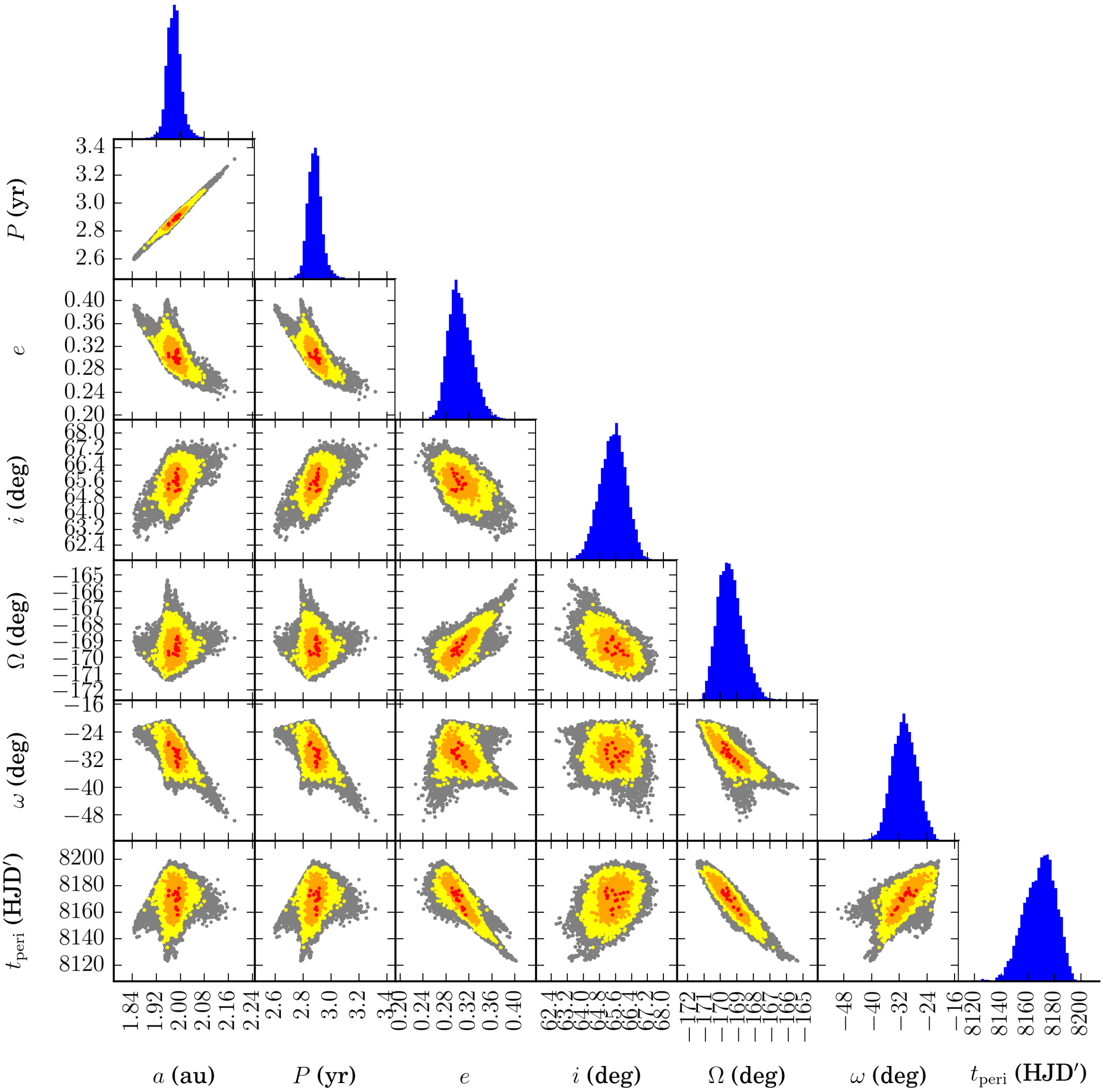

Fig. 9. Orbital elements of Gaia16aye. The panels show 2D and 1D projections of posterior distributions in the space of Kepler parameters. Red, orange, and yellow points mark 1σ, 2σ, and 3σ confidence regions, respectively.

to the angular size and hence to the lens mass measurement. We also note that the amount of the extinction derived based on our photometry ($A_V = 0.62$ mag) is significantly smaller than that measured by Schlafly & Finkbeiner (2011) in this direction ($A_V = 1.6$ mag). This and the uncertainty in the physical size of giant stars affects the estimate of the source distance, but because the lens is very nearby at less than 1 kpc, the source distance does not affect the overall result of this s study.

Nevertheless, an independent measurement of the Einstein radius, and thus the final confirmation of the nature of the lens in Gaia16aye, can be obtained in the near future from *Gaia* astrometric time-domain data. Using our photometry-based model, we computed the positions and amplifications of the images throughout the evolution of the event. Figure 10 shows the expected position of the combined light of all the images shown in the frame of the centre of mass of the binary and in units of the Einstein radius. The figure shows only the centroid motion due to microlensing relative to the unlensed position of the source. The moments of *Gaia* observations are marked with black dots. Because $\theta_{\rm E} = 3.04 \pm 0.24$ mas, the expected amplitude of the astrometric variation is about 3 mas. This should be detectable in *Gaia* astrometric time-series because *Gaia* is expected to have error bars in the along-scan direction of about 0.1 mas (Rybicki et al. 2018). The estimate of $\theta_{\rm E}$ from *Gaia* will be free of our assumptions about the intrinsic colours of the source and the interstellar extinction. The actual *Gaia* astrometry will also include the effects of parallax and proper motion of the source as well as the blended light from both components of the binary lens. The contribution of the lens brightness to the total light is about 25%, therefore the astrometric data might also be affected by the orbital motion of the binary. It is worth emphasising that without the microlensing model presented above, obtained from photometric *Gaia* and follow-up data alone, the interpretation of the *Gaia* astrometry will not be possible due to the high complexity of the centroid motion.

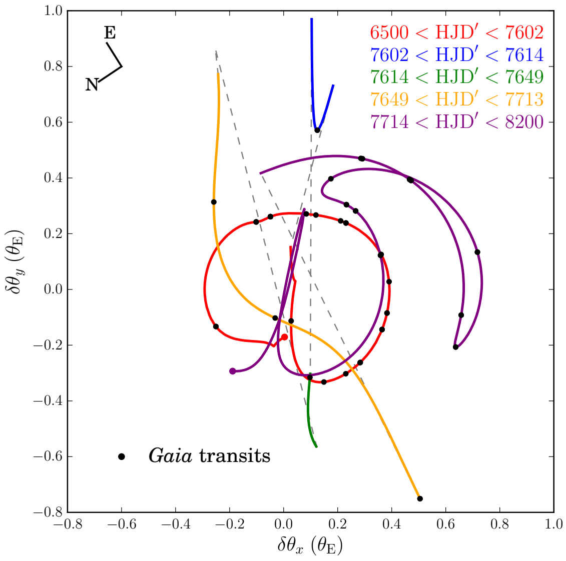

Fig. 10. As the source star moves across the caustics, new images of the source can be created while others may disappear, resulting in changes of the image centroid. Colour curves show the path of the centroid of the source images relative to the unlensed position of the source (additional light from components of the lens is not included). Moments of *Gaia* transits are marked with black points. The coordinate system is the same as in Fig. 7. The shifts are scaled to the angular Einstein radius of the system ($\theta_E = 3.04 \pm 0.24$ mas). Analysis of the *Gaia* astrometric measurements will provide an independent estimate of θ_E.

Radial velocity measurements of nearby binary lenses offer an additional way for post-event verification of the orbital parameters inferred from the microlensing model. So far, such an attempt was successfully achieved only in the case of OGLE-2009-BLG-020, a binary lens event with a clear orbital motion effect (Skowron et al. 2011). Follow-up observations from the Keck and Magellan telescopes measured the radial velocity of the binary to agree with the one predicted based on the microlensing event full binary lens orbit solution (Yee et al. 2016). The binary system presented in this work (to be denoted Gaia16aye-L, with its components Gaia16aye-La and Gaia16aye-Lb) is nearby (780 ± 60 pc) and fairly bright ($I \sim 16.5$ mag without the source star), hence such observations are obtainable. The expected amplitude of the radial velocity curve of the primary is about $K \approx 7.6\,\mathrm{km\,s^{-1}}$. We strongly encourage such observations to be carried out in order to verify the binary solution found in microlensing.

Yet another possibility to verify the model might come from AO or other high-resolution imaging techniques (e.g. Scott 2019) in some years when the source and the lens separate (e.g. Jung et al. 2018). With the relative proper motion of $10.1 \pm 0.8\,\mathrm{mas\,yr^{-1}}$, the binary lens should become visible at a separation of about 50 mas even in 2021.

6. Conclusions

We analysed the long-lasting event Gaia16aye, which exhibited four caustic crossings and a cusp approach, as well as space-parallax between the Earth and the *Gaia* spacecraft. The very well-sampled light curve allowed us to determine the masses of the binary system ($0.57 \pm 0.05\,M_\odot$ and $0.36 \pm 0.03\,M_\odot$) and all its orbital components. We derived the period (2.88 ± 0.05 years) and semi-major axis (1.98 ± 0.03 au), as well as the eccentricity of the orbit (0.30 ± 0.03). Gaia16aye is one of only a few microlensing binary systems with a full orbital solution, which offers an opportunity for confirming the binary parameters with radial velocity measurements and high-resolution imaging after some years. This event will also be detectable as an astrometric microlensing event in the forthcoming *Gaia* astrometric time-series data.

Increasingly more such events will be detectable in the current era of large-scale photometric surveys (e.g. *Gaia*, OGLE, ZTF). With the forthcoming thousands of alerts from all over the sky with the Large Synoptic Survey Telescope (LSST), it will become a necessity to use automated tools for transients discovery, their follow-up and follow-up data processing in order to fully identify and characterise the most interesting events. Robotic observations of selected alerts, automated analysis of the follow-up data, and light curve generation will soon become new standards in transient time-domain astronomy. The case of Gaia16aye shows that microlensing can be a useful tool for studying also binary systems where the lensing is caused by dark objects. A detection of a microlensing binary system composed of black holes and neutron stars would provide information about this elusive population of remnants that is complementary to other studies.

Acknowledgements. This work relies on the results from the European Space Agency (ESA) space mission *Gaia*. *Gaia* data are being processed by the *Gaia* Data Processing and Analysis Consortium (DPAC). Funding for the DPAC is provided by national institutions, in particular the institutions participating in the *Gaia* Multi-Lateral Agreement (MLA). The *Gaia* mission website is https://www.cosmos.esa.int/gaia. In particular we acknowledge *Gaia* Photometric Science Alerts Team, website http://gsaweb.ast.cam.ac.uk/alerts. We thank the members of the OGLE team for discussions and support. We also would like to thank the Polish Children Fund (KFnRD) for support of an internship of their pupils in Ostrowik Observatory of the Warsaw University, during which some of the data were collected, in particular we thank: Robert Nowicki, Michał Porębski and Karol Niczyj. The work presented here has been supported by the following grants from the Polish National Science Centre (NCN): HARMONIA NCN grant 2015/18/M/ST9/00544, OPUS NCN grant 2015/17/B/ST9/03167, DAINA NCN grant 2017/27/L/ST9/03221, as well as European Commission's FP7 and H2020 OPTICON grants (312430 and 730890), Polish Ministry of Higher Education support for OPTICON FP7, 3040/7.PR/2014/2, MNiSW grant DIR/WK/2018/12. PMr and JS acknowledge support from MAESTRO NCN grant 2014/14/A/ST9/00121 to Andrzej Udalski. We would like to thank the following members of the AAVSO for their amazing work with collecting vast amounts of data: Teofilo Arranz, James Boardman, Stephen Brincat, Geoff Chaplin, Emery Erdelyi, Rafael Farfan, William Goff, Franklin Guenther, Kevin Hills, Jens Jacobsen, Raymond Kneip, David Lane, Fernando Limon Martinez, Gianpiero Locatelli, Andrea Mantero, Attila Madai, Peter Meadows, Otmar Nickel, Arto Oksanen, Luis Perez, Roger Pieri, Ulisse Quadri, Diego Rodriguez Perez, Frank Schorr, George Sjoberg, Andras Timar, Ray Tomlin, Tonny Vanmunster, Klaus Wenzel, Thomas Wikander. We also thank the amateur observers from around the world, in particular, Pietro Capuozzo, Leone Trascianelli, Igor Zharkov from Ardingly College and Angelo Tomassini, Karl-Ludwig Bath. We also thank Roger Pickard from the British Astronomical Association and Matthias Penselin from the German Haus der Astronomie association for their contributions. KS thanks Dr. Dmitry Chulkov and Dr. Panagiotis Gavras for the interesting discussion of stellar multiplicity. We acknowledge support of DDT programmes SW2016b12 (WHT) and A34DDT3 (TNG). The INT, TNG and WHT are operated on the island of La Palma by the Isaac Newton Group of Telescopes in the Spanish Observatorio del Roque de los Muchachos of the Instituto de Astrofisica de Canarias. The Liverpool Telescope is operated on the island of La Palma by Liverpool John Moores University in the Spanish Observatorio del Roque de los Muchachos of the Instituto de Astrofisica de Canarias with financial support from the UK Science and Technology Facilities Council. SJF would like to thank the UCL students who assisted with the collection and checking of UCLO data for the observing campaign: Martina Aghopian, Ashleigh Arendt, Artem Barinov, Luke Barrett, Jasper Berry-Gair, Arjun Bhogal, Charles Bowesman, William Boyd, Andrei Cuceu, Michael Davies, Max Freedman, Gabriel Fu, Abirami Govindaraju, Iandeep Hothi, Clara Matthews Torres, Darius Modirrousta-Galian, Petru Neague, George Pattinson, Xiaoxi Song, and Brian Yu. P.Mr. acknowledges support from the Foundation for Polish Science (Program START) and the National Science Center, Poland (grant ETIUDA 2018/28/T/ST9/00096). AC, AG and NI acknowledge the financial support from the Slovenian Research Agency (research core funding No. P1-0031 and project grant No. J1-8136)

and networking support by the COST Action GWverse CA16104. Skinakas Observatory is a collaborative project of the University of Crete and the Foundation for Research and Technology-Hellas. Work by C.H. was supported by the grant (2017R1A4A1015178) of National Research Foundation of Korea. KW acknowledges funding from STFC, and thanks the University of Leicester for the investment in instrumentation. We gratefully acknowledge financial support by the European Space Agency under the NELIOTA program, contract No. 4000112943. This work has made use of data obtained with the Kryoneri Prime Focus Instrument, developed by the European Space Agency NELIOTA project on the 1.2 m Kryoneri telescope, which is operated by IAASARS, National Observatory of Athens, Greece. The Aristarchos telescope is operated on Helmos Observatory by the IAASARS of the National Observatory of Athens. This work was supported by the GROWTH project funded by the National Science Foundation under Grant No 1545949. This work was supported by the MINECO (Spanish Ministry of Economy) through grant ESP2016-80079-C2-1-R (MINECO/FEDER, UE) and ESP2014-55996-C2-1-R (MINECO/FEDER, UE) and MDM-2014-0369 of ICCUB (Unidad de Excelencia a María de Maeztu). This work was supported by the MINECO (Spanish Ministry of Economy) through grant ESP2016-80079-C2-1-R and RTI2018-095076-B-C21 (MINECO/FEDER, UE), and MDM-2014-0369 of ICCUB (Unidad de Excelencia 'María de Maeztu'). The *Joan Oró* Telescope (TJO) of the Montsec Astronomical Observatory (OAdM) is owned by the Catalan Government and is operated by the Institute for Space Studies of Catalonia (IEEC). Support to this study has been provided by Agenzia Spaziale Italiana (ASI) through grants ASI I/058/10/0 and ASI 2014-025-R.1.2015. KW thanks Dipali Thanki and Ray McErlean for their technical support of the scientific programme of the University of Leicester observatory. This work was supported by Royal Society Research Grant RG170230. CCN thanks the funding from Ministry of Science and Technology (Taiwan) under the contracts 104-2112-M-008-012-MY3 and 104-2923-M-008-004-MY5. The research leading to these results has received funding from the European Research Council under the European Union's Seventh Framework Programme (FP/2007-2013) / ERC Grant Agreement n. 320964 (WDTracer). We thank the Las Cumbres Observatory and its staff for its continuing support of the project. ASAS-SN is supported by the Gordon and Betty Moore Foundation through grant GBMF5490 to the Ohio State University and NSF grant AST-1515927. Development of ASAS-SN has been supported by NSF grant AST-0908816, the Mt. Cuba Astronomical Foundation, the Center for Cosmology and AstroParticle Physics at the Ohio State University, the Chinese Academy of Sciences South America Center for Astronomy (CAS- SACA), the Villum Foundation, and George Skestos. ARM acknowledges support from the MINECO under the Ramón y Cajal programme (RYC-2016-20254) and the AYA2017-86274-P grant, and the AGAUR grant SGR-661/2017. We acknowledge support from the Science and Technology Facilities Council (TB and RWW; ST/P000541/1). K.Horne acknowledges support from STFC consolidated grant ST/M001296/1. This work was partly supported by the Research Council of Lithuania, grant No. S-LL-19-2 Authors thank to TÜBİTAK, IKI, KFU, and AST for partial supports in using RTT150 (Russian-Turkish 1.5-m telescope in Antalya). This work was partially funded by the subsidy 3.6714.2017/8.9 allocated to Kazan Federal University for the state assignment in the sphere of scientific activities. This research was partially supported by contract DN 18/13-12.12.2017 with the National Science Fund (Bulgaria). Work by YS was supported by an appointment to the NASA Postdoctoral Program at the Jet Propulsion Laboratory, California Institute of Technology, administered by Universities Space Research Association through a contract with NASA. GD gratefully acknowledges the observing grant support from the Institute of Astronomy and NAO Rozhen, BAS, via bilateral joint research project "Study of ICRF radio-sources and fast variable astronomical objects" (PI:G.Damljanovic). This work is a part of the Projects no. 176011 "Dynamics and kinematics of celestial bodies and systems", no. 176004 "Stellar physics" and no. 176021 "Visible and invisible matter in nearby galaxies: theory and observations" supported by the Ministry of Education, Science and Technological Development of the Republic of Serbia. YT acknowledges the support of DFG priority program SPP 1992 "Exploring the diversity of Extrasolar Planets" (WA 1074/11-1). This work of PMi, DM and ZK was supported by the NCN grant no. 2016/21/B/ST9/01126. ARM acknowledges support from the MINECO Ramón y Cajal programme RYJ-2016-20254 and grant AYA2017-86274-P and from the AGAUR grant SGR-661/2017. The work by C. R. was supported by an appointment to the NASA Postdoctoral Program at the Goddard Space Flight Center, administered by USRA through a contract with NASA. The Faulkes Telescope Project is an education partner of Las Cumbres Observatory (LCO). The Faulkes Telescopes are maintained and operated by LCO. This research was made possible through the use of the AAVSO Photometric All-Sky Survey (APASS), funded by the Robert Martin Ayers Sciences Fund and NSF AST-1412587. The Pan-STARRS1 Surveys (PS1) and the PS1 public science archive have been made possible through contributions by the Institute for Astronomy, the University of Hawaii, the Pan-STARRS Project Office, the Max-Planck Society and its participating institutes, the Max Planck Institute for Astronomy, Heidelberg and the Max Planck Institute for Extraterrestrial Physics, Garching, The Johns Hopkins University, Durham University, the University of Edinburgh, the Queen's University Belfast, the Harvard-Smithsonian Center for Astrophysics, the Las Cumbres Observatory Global Telescope Network Incorporated, the National Central University of Taiwan, the Space Telescope Science Institute, the National Aeronautics and Space Administration under Grant No. NNX08AR22G issued through the Planetary Science Division of the NASA Science Mission Directorate, the National Science Foundation Grant No. AST-1238877, the University of Maryland, Eotvos Lorand University (ELTE), the Los Alamos National Laboratory, and the Gordon and Betty Moore Foundation. Some of the data presented herein were obtained at the W. M. Keck Observatory, which is operated as a scientific partnership among the California Institute of Technology, the University of California and the National Aeronautics and Space Administration. The Observatory was made possible by the generous financial support of the W. M. Keck Foundation.

References

Abbott, B. P., Abbott, R., Abbott, T. D., et al. 2016, Phys. Rev. X, 6, 041015
Abbott, B. P., Abbott, R., Abbott, T. D., et al. 2017, Phys. Rev. Lett., 118, 221101
Adams, A. D., Boyajian, T. S., & von Braun, K. 2018, MNRAS, 473, 3608
Albrow, M., Beaulieu, J.-P., Birch, P., et al. 1998, ApJ, 509, 687
Albrow, M. D., Beaulieu, J.-P., Caldwell, J. A. R., et al. 2000, ApJ, 534, 894
Alcock, C., Allsman, R. A., Alves, D., et al. 1997, ApJ, 479, 119
An, J. H., & Gould, A. 2001, ApJ, 563, L111
Asplund, M., Grevesse, N., Sauval, A. J., & Scott, P. 2009, ARA&A, 47, 481
Bachelet, E., Beaulieu, J.-P., Boisse, I., Santerne, A., & Street, R. A. 2018, ApJ, 865, 162
Bakis, V., Burgaz, U., Butterley, T., et al. 2016, ATel, 9376
Beaulieu, J.-P., Bennett, D. P., Fouqué, P., et al. 2006, Nature, 439, 437
Belczynski, K., Holz, D. E., Bulik, T., & O'Shaughnessy, R. 2016, Nature, 534, 512
Belokurov, V. A., & Evans, N. W. 2002, MNRAS, 331, 649
Bennett, D. P., Rhie, S. H., Udalski, A., et al. 2016, AJ, 152, 125
Bertin, E., & Arnouts, S. 1996, A&AS, 117, 393
Bird, S., Cholis, I., Muñoz, J. B., et al. 2016, Phys. Rev. Lett., 116, 201301
Blanco-Cuaresma, S., Soubiran, C., Jofré, P., & Heiter, U. 2014, A&A, 566, A98
Boisse, I., Santerne, A., Beaulieu, J.-P., et al. 2015, A&A, 582, L11
Bond, I. A., Udalski, A., Jaroszyński, M., et al. 2004, ApJ, 606, L155
Bozza, V. 2001, A&A, 374, 13
Brown, T. M., Baliber, N., Bianco, F. B., et al. 2013, PASP, 125, 1031
Calchi Novati, S., & Scarpetta, G. 2016, ApJ, 824, 109
Cardelli, J. A., Clayton, G. C., & Mathis, J. S. 1989, ApJ, 345, 245
Cropper, M., Katz, D., Sartoretti, P., et al. 2018, A&A, 616, A5
Derue, F., Afonso, C., Alard, C., et al. 2001, A&A, 373, 126
Dominik, M., & Sahu, K. C. 2000, ApJ, 534, 213
Dong, S., Mérand, A., Delplancke-Ströbele, F., et al. 2019, ApJ, 871, 70
Dyck, H. M., Benson, J. A., van Belle, G. T., & Ridgway, S. T. 1996, AJ, 111, 1705
Evans, D. W., Riello, M., De Angeli, F., et al. 2018, A&A, 616, A4
Foreman-Mackey, D., Hogg, D. W., Lang, D., & Goodman, J. 2013, PASP, 125, 306
French, J., Hanlon, L., McBreen, B., et al. 2004, AIP Conf. Ser., 727, 741
Fukui, A., Abe, F., Ayani, K., et al. 2007, ApJ, 670, 423
Fukui, A., Suzuki, D., Koshimoto, N., et al. 2019, AJ, 158, 206
Gaia Collaboration (Prusti, T., et al.) 2016, A&A, 595, A1
Gaia Collaboration (Brown, A. G. A., et al.) 2018, A&A, 616, A1
Gaudi, B. S., Patterson, J., Spiegel, D. S., et al. 2008, ApJ, 677, 1268
Goudis, C., Hantzios, P., Boumis, P., et al. 2010, ASP Conf. Ser., 424, 422
Gould, A. 1992, ApJ, 392, 442
Gould, A. 1994, ApJ, 421, L75
Gould, A. 2000, ApJ, 542, 785
Gould, A., & Loeb, A. 1992, ApJ, 396, 104
Gould, A., Udalski, A., Monard, B., et al. 2009, ApJ, 698, L147
Gray, R. O., & Corbally, C. J. 1994, AJ, 107, 742
Hamadache, C., Le Guillou, L., Tisserand, P., et al. 2006, A&A, 454, 185
Han, C. 2008, ApJ, 681, 806
Hardy, L. K., Butterley, T., Dhillon, V. S., Littlefair, S. P., & Wilson, R. W. 2015, MNRAS, 454, 4316
Hodgkin, S. T., Wyrzykowski, Ł., Blagorodnova, N., & Koposov, S. 2013, Phil. Trans. R. Soc. London Ser. A, 371, 20120239
Hogg, D. W., Blanton, M., Lang, D., Mierle, K., & Roweis, S. 2008, ASP Conf. Ser., 394, 27
Houdashelt, M. L., Bell, R. A., Sweigart, A. V., & Wing, R. F. 2000, AJ, 119, 1424
Jaroszynski, M., Udalski, A., Kubiak, M., et al. 2004, Acta Astron., 54, 103
Jung, Y. K., Han, C., Udalski, A., et al. 2018, ApJ, 863, 22
Kains, N., Calamida, A., Sahu, K. C., et al. 2017, ApJ, 843, 145

Kalberla, P. M. W., Burton, W. B., Hartmann, D., et al. 2005, A&A, 440, 775
Khamitov, I., Bikmaev, I., Burenin, R., et al. 2016a, ATel, 9753
Khamitov, I., Bikmaev, I., Burenin, R., et al. 2016b, ATel, 9780
Kim, S.-L., Lee, C.-U., Park, B.-G., et al. 2016, J. Korean Astron. Soc., 49, 37
Kiraga, M., & Paczynski, B. 1994, ApJ, 430, L101
Kochanek, C. S., Shappee, B. J., Stanek, K. Z., et al. 2017, PASP, 129, 104502
Kolb, U., Brodeur, M., Braithwaite, N., & Minocha, S. 2018, Robot. Telesc. Stud. Res. Edu. Proc., 1, 127
Kozłowski, S., Woźniak, P. R., Mao, S., & Wood, A. 2007, ApJ, 671, 420
Kupka, F., Dubernet, M. L., & VAMDC Collaboration 2011, Baltic Astron., 20, 503
Kurucz, R. 1993, ATLAS9 Stellar Atmosphere Programs and 2 km/s grid. Kurucz CD-ROM No. 13 (Cambridge, MA: Smithsonian Astrophysical Observatory)
Lang, D., Hogg, D. W., Mierle, K., Blanton, M., & Roweis, S. 2010, AJ, 139, 1782
Lu, J. R., Sinukoff, E., Ofek, E. O., Udalski, A., & Kozlowski, S. 2016, ApJ, 830, 41
Mróz, P., Wyrzykowski, Ł., Rybicki, K., et al. 2016, ATel, 9770
Mróz, P., Udalski, A., Skowron, J., et al. 2017, Nature, 548, 183
Nesci, R. 2016, ATel, 9533
Nucita, A. A., Licchelli, D., De Paolis, F., et al. 2018, MNRAS, 476, 2962
Paczyński, B. 1971, ARA&A, 9, 183
Paczynski, B. 1996, ARA&A, 34, 419
Pecaut, M. J., & Mamajek, E. E. 2013, ApJS, 208, 9
Penny, M. T., Kerins, E., & Mao, S. 2011, MNRAS, 417, 2216
Pietrzyński, G., Thompson, I. B., Gieren, W., et al. 2010, Nature, 468, 542
Poleski, R., Skowron, J., Udalski, A., et al. 2014, ApJ, 795, 42
Poleski, R., Zhu, W., Christie, G. W., et al. 2016, ApJ, 823, 63
Popowski, P., Alcock, C., Allsman, R. A., et al. 2001, ASP Conf. Ser., 239, 244
Popper, D. M. 1967, ARA&A, 5, 85
Rahal, Y. R., Afonso, C., Albert, J. N., et al. 2009, A&A, 500, 1027
Rattenbury, N. J. 2009, MNRAS, 392, 439
Refsdal, S. 1966, MNRAS, 134, 315
Rybicki, K. A., Wyrzykowski, Ł., Klencki, J., et al. 2018, MNRAS, 476, 2013
Sahu, K. C., Anderson, J., Casertano, S., et al. 2017, Am. Astron. Soc. Meet. Abstr., 230, 315.13
Sartoretti, P., Katz, D., Cropper, M., et al. 2018, A&A, 616, A6
Schlafly, E. F., & Finkbeiner, D. P. 2011, ApJ, 737, 103
Scott, N. J. 2019, AAS/Division Extreme Sol. Syst. Abstr., 51, 330.15
Shappee, B. J., Prieto, J. L., Grupe, D., et al. 2014, ApJ, 788, 48
Shin, I.-G., Han, C., Choi, J.-Y., et al. 2012, ApJ, 755, 91
Shvartzvald, Y., Udalski, A., Gould, A., et al. 2015, ApJ, 814, 111
Shvartzvald, Y., Li, Z., Udalski, A., et al. 2016, ApJ, 831, 183
Skowron, J., Jaroszynski, M., Udalski, A., et al. 2007, Acta Astron., 57, 281
Skowron, J., Wyrzykowski, Ł., Mao, S., & Jaroszyński, M. 2009, MNRAS, 393, 999
Skowron, J., Udalski, A., Gould, A., et al. 2011, ApJ, 738, 87
Sokolovsky, K., Korotkiy, S., & Lebedev, A. 2014, ASP Conf. Ser., 490, 395
Steele, I. A., Smith, R. J., Rees, P. C., et al. 2004, Proc. SPIE, 5489, 679
Stetson, P. B. 1987, PASP, 99, 191
Sumi, T., Bennett, D. P., Bond, I. A., et al. 2013, ApJ, 778, 150
Udalski, A., Szymanski, M., Stanek, K. Z., et al. 1994a, Acta Astron., 44, 165
Udalski, A., Szymanski, M., Mao, S., et al. 1994b, ApJ, 436, L103
Udalski, A., Zebrun, K., Szymanski, M., et al. 2000, Acta Astron., 50, 1
Udalski, A., Jaroszyński, M., Paczyński, B., et al. 2005, ApJ, 628, L109
Udalski, A., Szymański, M. K., & Szymański, G. 2015a, Acta Astron., 65, 1
Udalski, A., Yee, J. C., Gould, A., et al. 2015b, ApJ, 799, 237
Udalski, A., Han, C., Bozza, V., et al. 2018, ApJ, 853, 70
Villanueva, Jr., S., Gaudi, B. S., Pogge, R. W., et al. 2018, PASP, 130, 015001
Witt, H. J., & Mao, S. 1995, ApJ, 447, L105
Wozniak, P. R., Udalski, A., Szymanski, M., et al. 2001, Acta Astron., 51, 175
Wyrzykowski, Ł., & Hodgkin, S. 2012, IAU Symp., 285, 425
Wyrzykowski, Ł., Hodgkin, S., Blogorodnova, N., Koposov, S., & Burgon, R. 2012, 2nd Gaia Follow-up Network for Solar System Objects, 21
Wyrzykowski, Ł., Hodgkin, S., & Blagorodnova, N. 2014, Gaia-FUN-SSO-3, 31
Wyrzykowski, Ł., Rynkiewicz, A. E., Skowron, J., et al. 2015, ApJS, 216, 12
Wyrzykowski, Ł., Kostrzewa-Rutkowska, Z., Skowron, J., et al. 2016, MNRAS, 458, 3012
Wyrzykowski, Ł., Mroz, P., Rybicki, K., et al. 2017, ATel, 10341
Xilouris, E. M., Bonanos, A. Z., Bellas-Velidis, I., et al. 2018, A&A, 619, A141
Yee, J. C. 2015, ApJ, 814, L11
Yee, J. C., Udalski, A., Calchi Novati, S., et al. 2015, ApJ, 802, 76
Yee, J. C., Johnson, J. A., Skowron, J., et al. 2016, ApJ, 821, 121
Yock, P. C. M. 1998, in Frontiers Science Series 23: Black Holes and High Energy Astrophysics, eds. H. Sato, & N. Sugiyama, 375
Yoo, J., DePoy, D. L., Gal-Yam, A., et al. 2004, ApJ, 603, 139
Zhu, W., Calchi Novati, S., Gould, A., et al. 2016, ApJ, 825, 60
Zieliński, P., Wyrzykowski, Ł., Rybicki, K., et al. 2019, Contrib. Astron. Obs. Skalnate Pleso, 49, 125
Zub, M., Cassan, A., Heyrovský, D., et al. 2011, A&A, 525, A15

[1] Warsaw University Astronomical Observatory, Al. Ujazdowskie 4, 00-478 Warszawa, Poland
e-mail: wyrzykow@astrouw.edu.pl
[2] Department of Physics, Chungbuk National University, Cheongju 28644, Republic of Korea
[3] Sternberg Astronomical Institute, Moscow State University, Universitetskii pr. 13, 119992 Moscow, Russia
[4] Instituto de Astrofisica de Canarias (IAC), 38205 La Laguna, Tenerife, Spain
[5] Universidad de La Laguna, Dpto. Astrofísica, 38206 La Laguna, Tenerife, Spain
[6] Institute of Astronomy, University of Cambridge, Madingley Road, CB3 0HA Cambridge, UK
[7] INAF – Osservatorio Astronomico di Roma, Via di Frascati 33, 00078 Monte Porzio Catone, Roma, Italy
[8] Indian Institute of Astrophysics, II Block Koramangala, Bengaluru 560034, India
[9] National Astronomical Research Institute of Thailand, 260, Moo 4, T. Donkaew, A. Mae Rim, Chiang Mai 50180, Thailand
[10] Department of Space Sciences and Technologies, Faculty of Science, Akdeniz University, 07058, Antalya, Turkey
[11] Université Côte d'Azur, Observatoire de la Côte d'Azur, CNRS, Laboratoire Lagrange, France
[12] School of Physics and Astronomy, Tel-Aviv University, Tel-Aviv 6997801, Israel
[13] Jet Propulsion Laboratory, California Institute of Technology, 4800 Oak Grove Drive, Pasadena, CA 91109, USA
[14] Harvard-Smithsonian Center for Astrophysics, 60 Garden Street, Cambridge, MA 02138, USA
[15] Institute of Astronomy and NAO Rozhen, BAS, 72 Tsarighradsko Shousse Blvd., 1784 Sofia, Bulgaria
[16] National Optical Astronomy Observatory, 950 N Cherry Avenue, Tucson, AZ 85719, USA
[17] Subaru Telescope, National Astronomical Observatory of Japan, 650 N Aohoku Place, Hilo, HI 96720, USA
[18] IAASARS, National Observatory of Athens, Vas. Pavlou & I. Metaxa, 15236 Penteli, Greece
[19] Dipartimento di Fisica E.R. Caianiello, Università di Salerno, Via Giovanni Paolo II 132, 84084 Fisciano, SA, Italy
[20] Department of Astronomy and Space Sciences, Ege University, 35100 Izmir, Turkey
[21] Centre for Advanced Instrumentation, University of Durham, South Road, Durham DH1 3LE, UK
[22] Institut del Ciències del Cosmos (ICC), Universitat de Barcelona (IEEC-UB), c/ Martí i Franquès, 1, 08028 Barcelona, Spain
[23] Department of Astrophysics/IMAPP, Radboud University Nijmegen, PO Box 9010, 6500 Nijmegen, The Netherlands
[24] INAF – Osservatorio di Astrofisica e Scienza dello Spazio di Bologna, Via Gobetti 93/3, 40129 Bologna, Italy
[25] Astronomical Observatory, Volgina 7, 11060 Belgrade, Serbia
[26] Science Support Office, Directorate of Science, European Space Research and Technology Centre (ESA/ESTEC), Keplerlaan 1, 2201 Noordwijk, The Netherlands
[27] Qatar Environment and Energy Research Institute(QEERI), HBKU, Qatar Foundation, Doha, Qatar
[28] Institut d'Astrophysique de Paris, Sorbonne Université, CNRS, UMR 7095, 98 bis bd Arago, 75014 Paris, France
[29] Department of Physics and Astronomy, University of Sheffield, Sheffield S3 7RH, UK
[30] Centre for Exoplanet Science, SUPA School of Physics & Astronomy, University of St Andrews, North Haugh, St Andrews KY16 9SS, UK
[31] Akdeniz University, Dumlupinar Blv., Campus, 07058 Antalya, Turkey
[32] Istanbul University, Department of Astronomy and Space Sciences, 34119, Beyazit Istanbul, Turkey

[33] Dept. of Physics & Astronomy, UCL, Gower St., London WC1E 6BT, UK
[34] Center for Astrophysics and Cosmology, University of Nova Gorica, Vipavska cesta 11c, 5270 Ajdovščina, Slovenia
[35] European Southern Observatory, Karl Schwarzschild Str 2, 85748 Garching, Germany
[36] Astronomical Observatory, Jagiellonian University, Kraków, Poland
[37] Mt. Suhora Observatory, Pedagogical University, ul. Podchor ażych 2, 30-084 Kraków, Poland
[38] Astronomical Institute of the Academy of Sciences of the Czech Republic, Ondřejov, Czech Republic
[39] Czech Technical University, Faculty of Electrical Engineering, Technická 2. 166 27, Praha 6, Czech Republic
[40] Zentrum für Astronomie der Universität Heidelberg, Astronomisches Rechen-Institut, Mönchhofstr. 12-14, 69120 Heidelberg, Germany
[41] International Space Science Institute, Hallerstrasse 6, 3012 Bern, Switzerland
[42] Department of Physics, School of Science, Tokyo Institute of Technology, 2-12-1 Ohokayama, Meguro, Tokyo 152-8551, Japan
[43] TÜBİTAK National Observatory, Akdeniz University Campus, 07058 Antalya, Turkey
[44] Instytut Astronomiczny Uniwersytetu Wrocławskiego, ul. Kopernika 11, 51-622 Wrocław, Poland
[45] Institute for Astronomy, University of Edinburgh, Royal Observatory, Edinburgh EH9 3HJ, UK
[46] School of Physical Sciences, The Open University, Walton Hall, Milton Keynes MK7 6AA, UK
[47] Osservatorio Astronomico Provinciale di Montarrenti, S. S. 73 Ponente, 53018, Sovicille Siena, Italy
[48] INAF – Osservatorio Astrofisico di Catania, Via Santa Sofia 78, 95123 Catania, Italy
[49] Faulkes Telescope Project, School of Physics, and Astronomy, Cardiff University, The Parade, Cardiff CF24 3AA, UK
[50] Astronomy Department, University of California, Berkeley, CA 94720, USA
[51] Department of Physics, University of Warwick, Coventry CV4 7AL, UK
[52] National Astronomical Observatories, Chinese Academy of Sciences, 100012 Beijing, PR China
[53] Graduate Institute of Astronomy, National Central University, Jhongli 32001, Taiwan
[54] Department of particle physics and astrophysics, Weizmann Institute of Science, Revovot, Israel
[55] Institute of Theoretical Physics and Astronomy, Vilnius University, Saulėtekio Av. 3, 10257 Vilnius, Lithuania
[56] Department of Astronomy, Ohio State University, 140 W. 18th Ave., Columbus, OH 43210, USA
[57] Soka University of America, 1 University Drive, Aliso Viejo, CA 92656, USA
[58] Astrophysics Research Institute, Liverpool John Moores University, 146 Brownlow Hill, Liverpool L3 5RF, UK
[59] Universitat Politècnica de Catalunya, Departament de Física, c/Esteve Terrades 5, 08860 Castelldefels, Spain
[60] Institute of Astrophysics, Foundation for Research and Technology-Hellas, 71110 Heraklion, Crete, Greece
[61] New York University Abu Dhabi, Saadiyat Island, PO Box 129188, Abu Dhabi, UAE
[62] Las Cumbres Observatory Global Telescope Network, 6740 Cortona Drive, Suite 102, Goleta, CA 93117, USA
[63] INAF Osservatorio Astronomico di Padova, Vicolo dell'Osservatorio 5, 35122 Padova, Italy
[64] Institute of Theoretical Physics, Faculty of Mathematics and Physics, Charles University, Prague, Czech Republic
[65] Astro Space Center of Lebedev Physical Institute, Profsoyuznaya St. 84/32, 117997 Moscow, Russia
[66] INAF – Istituto di Astrofisica e Planetologia Spaziali, Roma, Italy
[67] Department of Physics and Astronomy, University of Leicester, University Road, Leicester LE1 7RH, UK
[68] Institute for Astronomy, University of Hawai'i, 2680 Woodlawn Drive, Honolulu, HI 96822, USA
[69] Astrophysics Science Division, NASA/Goddard Space Flight Center, Greenbelt, MD 20771, USA
[70] Institute for Space Studies of Catalonia, c/Gran Capitá 2–4, Edif. Nexus 104, 08034 Barcelona, Spain
[71] Space Science Data Center – ASI, Via del Politecnico SNC, 00133 Roma, Italy
[72] Institute of Astronomy, Russian Academy of Sciences, Pyatnitskaya str. 48, 119017 Moscow, Russia
[73] Observatoire de Genève, Université de Genève, 1290 Versoix, Switzerland
[74] University of Crete, Physics Department & Institute of Theoretical & Computational Physics, 71003 Heraklion, Crete, Greece
[75] Kazan Federal University, ul. Kremlevskaya 18, 420008 Kazan, Russia
[76] Center for Theoretical Physics, Polish Academy of Sciences, Al. Lotników 32/46, 02-668 Warsaw, Poland
[77] Department of Astrophysics, Astronomy & Mechanics, Faculty of Physics, University of Athens, 15783 Athens, Greece
[78] Nicolaus Copernicus Astronomical Center, Polish Academy of Sciences, ul. Bartycka 18, 00-716 Warsaw, Poland
[79] Istituto Nazionale di Fisica Nucleare, Sezione di Napoli, Italy
[80] Instituto de Astrofísica, Facultad de Física, Pontificia Universidad Católica de Chile, Av. Vicuña Mackenna 4860, 7820436, Macul Santiago, Chile
[81] Istituto Internazionale per gli Alti Studi Scientifici (IIASS), Via G. Pellegrino 19, 84019 Vietri sul Mare, SA, Italy
[82] IPAC, Mail Code 100-22, California Institute of Technology, 1200 East California Boulevard, Pasadena, CA 91125, USA
[83] Space Research Institute of Russian Academy of Sciences (IKI), 84/32 Profsoyuznaya, Moscow, Russia
[84] National Research University Higher School of Economics, Myasnitskaya ul. 20, 101000 Moscow, Russia
[85] Institute of Solar-Terrestrial Physics SB RAS, Irkutsk, Russia
[86] Academy of Sciences of Tatarstan, Kazan, Russia
[87] Kavli Institute for Cosmology, Madingley Road, Cambridge CB3 0HA, UK
[88] Université Côte d'Azur, OCA, CNRS, Laboratoire Lagrange, Nice, France
[89] Crimean Astrophysical Observatory, Nauchnyi, Crimea
[90] American Association of Variable Star Observers (AAVSO), 49 Bay State Road, Cambridge, MA 02138, USA
[91] Swarthmore College, 500 College Avenue, Swarthmore, PA 19081, USA
[92] Dark Sky Observatory, Department of Physics and Astronomy, Appalachian State University, Boone, NC 28608, USA
[93] University of North Carolina, Chapel Hill, North Carolina, NC 27599, USA
[94] Yerkes Observatory, Department of Astronomy and Astrophysics, University of Chicago, 373 W. Geneva St., Williams Bay, WI 53191, USA
[95] Núcleo de Astronomía de la Facultad de Ingeniería, Universidad Diego Portales, Av. Ejército 441, Santiago, Chile
[96] Millenium Institute of Astrophysics, Santiago, Chile
[97] Horten Upper Secondary School, Bekkegata 2, 3181 Horten, Norway
[98] Aryabhatta Research Institute of Observational Sciences (ARIES), Manora Peak, Nainital 263002, India
[99] Mullard Space Science Laboratory, University College London, Holmbury St Mary, Dorking RH5 6NT, UK
[100] GEPI, Observatoire de Paris, Université PSL, CNRS, 5 Place Jules Janssen, 92190 Meudon, France
[101] School of Physics, University College Dublin, Belfield, Dublin 4, Ireland
[102] Department of Physics, Faculty of Natural and Agricultural Sciences, University of the Free State, Bloemfontein 9300, Republic of South Africa

Appendix A: Parameters of the telescopes taking part in the follow-up

Table A.1 lists the instruments that were used in all telescopes that took part in the photometric follow-up of the Gaia16aye binary microlensing event.

Table A.1. Photometric instruments used in the follow-up observations of Gaia16aye.

Telescope code	Mirror size [m]	Instrument	Pixel scale [arcsec]
AAVSO	–	–	–
Akeno50	0.5	3 × Apogee Alta U6	1.64
APT2	0.8	e2v CCD230-42	0.93
Aries130	1.30	CCD Andor DZ436	0.54
Aristarchos	2.3	VersArray 2048B	0.16
ASASSN	0.14	FLI ProLine230	7.80
ASV1	0.6	SBIG ST10 XME	0.23
		Apogee Alta E47	0.45
ASV2	1.4	Apogee Alta U42	0.24
AUT25	0.25	QSI532swg	0.71
BAS2	2.0	CCD VersArray 1300B	0.74
		Photometrics for FoReRo2 system	0.88
BAS50/70	0.5/0.7	FLI ProLine16803	1.08
Bialkow	0.6	Andor iKon DW432-BV	0.61
C2PU	1.04	SBIG ST16803	0.56
Conti	0.28	SX694 mono CCD	0.56
CrAO	0.2	SBIG ST8300M	1.10
DEMONEXT	0.5	Fairchild CCD3041 $2k \times 2k$ array	0.90
Foligno	0.3	Nikon D90	0.76
HAO50	0.5	ATIK314+	0.67
Krakow50	0.5	Apogee Alta U42	0.42
Kryoneri	1.2	Andor Zyla 5.5	0.40
LCO-Texas	1.0	Sinistro $4k \times 4k$	0.39
LCO-Hawaii	0.4	SBIG STL-6303 $3k \times 2k$	1.14
	2.0	Spectral $4k \times 4k$	0.30
Leicester	0.5	SBIG ST2000XM (before 2017 Nov.)	0.89
		Moravian G3-11000 (after 2017 Nov.)	1.08
Loiano	1.52	BFOSC	0.58
LOT1m	1.0	Apogee Alta U42	0.35
LT	2.0	IO:O e2v CCD231	0.27
MAO165	1.65	Apogee Alta U47	0.51
Mercator	1.2	Merope	0.19
Montarrenti	0.53	Apogee Alta U47	1.16
OHP	1.2	$1k \times 1k$ CCD	0.67
OndrejovD50	0.5	CCD FLI IMG 4710	1.18
Ostrowik	0.6	CCD 512 × 512 Tektronix	0.76
PIRATE	0.42	FLI ProLine16803	0.63
pt5m	0.5	QSI532 CCD	0.28
RTT150	1.5	TFOSC	0.39
SAI	0.6	Apogee Aspen CG42	0.76
Salerno	0.6	FLI ProLine230	0.60
SKAS-KFU28	0.28	QSI 583wsg	0.40
Skinakas	1.3	Andor DZ436	0.28
SKYNET	1.0	512 × 512 CCD 48um	1.21
Swarthmore24	0.6	Apogee Alta U16M	0.38
T60	0.6	FLI ProLine3041	0.51
T100	1.0	$4k \times 4k$ CCD	0.31
TJO	0.8	MEIA e2V CCD42-40	0.36
TRT-GAO	0.7	Andor iKon-L 936	0.61
TRT-TNO	0.5	Andor iKon-L 936	0.68
UCLO-C14E	0.35	SBIG STL6303E	0.86
UCLO-C14W	0.35	SBIG STL6303E	0.86
UBT60	0.6	Apogee Alta U47	0.68
Watcher	0.4	Andor iXon EM+	0.60
WHT-ACAM	4.2	ACAM	0.25
Wise1m	1.0	PI camera	0.58
WiseC28	0.71	FLI ProLine16801	0.83

Appendix B: *Gaia* photometry

Table B.1 contains all *Gaia* mean G-band photometry for the Gaia16aye event that was collected and calibrated by the *Gaia* Science Alerts system, available online[6]. The typical error bar is about 0.1 mag.

Table B.1. *Gaia* photometric measurements of the Gaia16aye microlensing event.

Observation date		Average
TCB	JD	G mag
2014-10-30 20:50:59	2456961.369	15.48
2014-10-30 22:37:33	2456961.443	15.48
2015-02-15 09:54:03	2457068.913	15.44
2015-02-15 14:07:43	2457069.089	15.44
2015-02-15 15:54:18	2457069.163	15.45
2015-03-09 08:16:20	2457090.845	15.45
2015-03-09 10:02:55	2457090.919	15.43
2015-03-09 14:16:35	2457091.095	15.45
2015-03-09 16:03:10	2457091.169	15.45
2015-05-20 19:20:37	2457163.306	15.45
2015-06-10 03:08:39	2457183.631	15.47
2015-07-25 13:45:22	2457229.073	15.45
2015-08-04 00:05:24	2457238.504	15.45
2015-08-04 01:51:58	2457238.578	15.46
2015-10-08 06:23:08	2457303.766	15.40
2015-11-11 05:44:30	2457337.739	15.35
2015-12-18 09:29:34	2457374.896	15.35
2015-12-18 11:16:08	2457374.970	15.35
2016-01-08 03:37:06	2457395.651	15.35
2016-01-08 05:23:40	2457395.725	15.35
2016-01-08 09:37:20	2457395.901	15.39
2016-01-08 11:23:54	2457395.975	15.34
2016-02-27 21:18:55	2457446.388	15.48
2016-02-27 23:05:29	2457446.462	15.38
2016-02-28 03:19:09	2457446.638	15.39
2016-03-23 23:08:54	2457471.465	15.40
2016-04-25 22:50:35	2457504.452	15.39
2016-06-02 20:18:57	2457542.346	15.52
2016-06-20 04:10:13	2457559.674	15.23
2016-08-05 00:53:51	2457605.537	14.18
2016-08-05 02:40:25	2457605.611	14.19
2016-08-05 06:54:05	2457605.788	14.40
2016-08-05 08:40:39	2457605.862	14.25
2016-08-15 13:00:28	2457616.042	15.26
2016-08-15 14:47:02	2457616.116	15.05
2016-09-27 13:28:36	2457659.062	13.67
2016-10-21 05:33:20	2457682.731	14.09
2016-11-21 17:05:46	2457714.212	12.81
2016-11-21 18:52:20	2457714.286	13.00
2017-01-02 12:24:22	2457756.017	14.91
2017-01-02 16:38:01	2457756.193	14.94
2017-01-02 18:24:35	2457756.267	14.91
2017-01-20 10:48:21	2457773.950	14.75
2017-01-20 12:34:55	2457774.024	14.77
2017-01-20 16:48:35	2457774.200	14.75
2017-01-20 18:35:09	2457774.274	14.78
2017-03-10 23:52:28	2457823.495	14.53

Table B.1. continued.

Observation date		Average
TCB	JD	G mag
2017-03-11 01:39:02	2457823.569	14.56
2017-04-07 23:48:22	2457851.492	14.45
2017-04-08 01:34:57	2457851.566	14.47
2017-05-07 11:34:44	2457880.982	13.96
2017-05-07 13:21:19	2457881.056	13.98
2017-06-16 16:39:01	2457921.194	14.87
2017-08-16 09:12:15	2457981.884	15.26
2017-08-16 10:58:49	2457981.958	15.27
2017-08-28 17:04:45	2457994.212	15.32
2017-08-28 21:18:24	2457994.388	15.29
2017-10-08 14:08:21	2458035.089	15.4
2017-10-08 15:54:55	2458035.163	15.41
2017-11-04 03:39:50	2458061.653	15.55
2017-12-03 09:23:18	2458090.891	15.53
2018-01-18 19:12:05	2458137.300	15.53
2018-01-18 20:58:40	2458137.374	15.53
2018-01-19 01:12:20	2458137.550	15.52
2018-01-19 07:12:33	2458137.800	15.54
2018-02-04 19:23:34	2458154.308	15.52
2018-02-04 21:10:08	2458154.382	15.51
2018-02-05 01:23:49	2458154.558	15.51
2018-02-05 03:10:23	2458154.632	15.51
2018-03-23 01:03:21	2458200.544	15.54
2018-04-22 12:49:53	2458231.035	15.54
2018-04-22 14:36:27	2458231.109	15.56
2018-05-19 00:41:48	2458257.529	15.53
2018-06-30 07:22:25	2458299.807	15.56
2018-07-12 01:29:24	2458311.562	15.58
...	...	

Notes. TCB is the barycentric coordinate time. The full table is available at the CDS.

[6] http://gsaweb.ast.cam.ac.uk/alerts/alert/Gaia16aye

Appendix C: Photometric follow-up data

Photometric follow-up observations calibrated with the Cambridge Photometric Calibration Server are gathered in Table C.1. The complete table is available at the CDS.

Table C.1. Photometric follow-up observations of Gaia16aye.

ID	MJD [d]	Magnitude [mag]	Error [mag]	Filter	Observatory/Observer
41329	57609.74664	16.635	0.052	*B*	UBT60 V.Bakis
41348	57609.74742	14.914	0.012	*V*	UBT60 V.Bakis
41367	57609.74819	14.108	0.006	*r*	UBT60 V.Bakis
41386	57609.74897	13.375	0.005	*i*	UBT60 V.Bakis
41330	57609.74978	16.548	0.037	*B*	UBT60 V.Bakis
41349	57609.75055	14.907	0.010	*V*	UBT60 V.Bakis
41368	57609.75133	14.102	0.005	*r*	UBT60 V.Bakis
41387	57609.75210	13.378	0.005	*i*	UBT60 V.Bakis
41331	57609.75281	16.600	0.037	*B*	UBT60 V.Bakis
41350	57609.75359	14.897	0.010	*V*	UBT60 V.Bakis
41369	57609.75436	14.117	0.005	*r*	UBT60 V.Bakis
41388	57609.75514	13.374	0.005	*i*	UBT60 V.Bakis
41332	57609.75588	16.504	0.035	*B*	UBT60 V.Bakis
41351	57609.75665	14.902	0.010	*V*	UBT60 V.Bakis
41370	57609.75743	14.105	0.005	*r*	UBT60 V.Bakis
41389	57609.75820	13.399	0.005	*i*	UBT60 V.Bakis
41333	57609.75896	16.538	0.035	*B*	UBT60 V.Bakis
41352	57609.75973	14.904	0.010	*V*	UBT60 V.Bakis
41371	57609.76051	14.117	0.006	*r*	UBT60 V.Bakis
41390	57609.76128	13.403	0.005	*i*	UBT60 V.Bakis
54690	57609.78240	14.202	0.009	*r*	SAI A.Zubareva
54689	57609.78569	16.528	0.024	*B*	SAI A.Zubareva
54680	57609.78902	16.544	0.016	*B*	SAI A.Zubareva
54663	57609.79078	14.974	0.007	*V*	SAI A.Zubareva
54681	57609.79218	14.148	0.005	*r*	SAI A.Zubareva
54682	57609.79395	16.539	0.019	*B*	SAI A.Zubareva
41334	57609.79522	16.599	0.024	*B*	UBT60 V.Bakis
54664	57609.79569	14.971	0.008	*V*	SAI A.Zubareva
41353	57609.79600	14.884	0.008	*V*	UBT60 V.Bakis
41372	57609.79677	14.082	0.005	*r*	UBT60 V.Bakis
54683	57609.79711	14.167	0.005	*r*	SAI A.Zubareva
41391	57609.79755	13.355	0.005	*i*	UBT60 V.Bakis
54684	57609.79888	16.583	0.020	*B*	SAI A.Zubareva
54665	57609.80063	15.014	0.009	*V*	SAI A.Zubareva
54685	57609.80202	14.168	0.005	*r*	SAI A.Zubareva
54686	57609.80373	14.178	0.005	*r*	SAI A.Zubareva
41335	57609.80477	16.605	0.026	*B*	UBT60 V.Bakis
41354	57609.80554	14.876	0.008	*V*	UBT60 V.Bakis
41373	57609.80632	14.102	0.005	*r*	UBT60 V.Bakis
41392	57609.80709	13.374	0.005	*i*	UBT60 V.Bakis
41336	57609.80787	16.549	0.025	*B*	UBT60 V.Bakis
41355	57609.80864	14.864	0.008	*V*	UBT60 V.Bakis
41374	57609.80942	14.106	0.005	*r*	UBT60 V.Bakis
41393	57609.81019	13.380	0.005	*i*	UBT60 V.Bakis
41337	57609.81094	16.488	0.025	*B*	UBT60 V.Bakis
41356	57609.81171	14.884	0.008	*V*	UBT60 V.Bakis
41375	57609.81249	14.102	0.005	*r*	UBT60 V.Bakis
41394	57609.81326	13.382	0.005	*i*	UBT60 V.Bakis
41338	57609.81405	16.492	0.027	*B*	UBT60 V.Bakis
41357	57609.81483	14.879	0.008	*V*	UBT60 V.Bakis
41376	57609.81560	14.101	0.005	*r*	UBT60 V.Bakis
41395	57609.81638	13.374	0.005	*i*	UBT60 V.Bakis
40186	57609.90821	17.158	0.134	*B*	pt5m L.Hardy
40187	57609.90927	16.939	0.116	*B*	pt5m L.Hardy
40188	57609.91009	16.548	0.098	*B*	pt5m L.Hardy
40189	57609.91092	14.917	0.022	*V*	pt5m L.Hardy
40190	57609.91181	14.964	0.021	*V*	pt5m L.Hardy
40191	57609.91263	14.958	0.022	*V*	pt5m L.Hardy
40192	57609.91346	14.132	0.009	*r*	pt5m L.Hardy
40193	57609.91457	14.188	0.011	*r*	pt5m L.Hardy
40194	57609.91540	14.106	0.010	*r*	pt5m L.Hardy
40195	57609.91640	13.439	0.010	*i*	pt5m L.Hardy
40196	57609.91751	13.448	0.009	*i*	pt5m L.Hardy
40197	57609.91834	13.453	0.010	*i*	pt5m L.Hardy
40268	57610.00399	16.522	0.014	*B*	TJO U.Burgaz
40271	57610.01489	15.002	0.006	*V*	TJO U.Burgaz
40272	57610.01842	14.956	0.020	*V*	TJO U.Burgaz
40274	57610.03669	13.107	0.055	*i*	TJO U.Burgaz
40275	57610.04022	13.293	0.011	*i*	TJO U.Burgaz
40276	57610.04375	13.388	0.004	*i*	TJO U.Burgaz
54687	57610.05719	16.491	0.057	*B*	SAI A.Zubareva
54666	57610.05894	14.977	0.018	*V*	SAI A.Zubareva
54688	57610.06035	14.192	0.009	*r*	SAI A.Zubareva
41339	57610.76348	16.499	0.029	*B*	UBT60 V.Bakis
41358	57610.76424	14.805	0.009	*V*	UBT60 V.Bakis
41377	57610.76499	14.009	0.005	*r*	UBT60 V.Bakis
41396	57610.76576	13.285	0.005	*i*	UBT60 V.Bakis
…	…	…	…	.	…

Table C.1. continued.

Notes. ID denotes the unique id of the observation in the Calibration Server. The full table is available at the CDS.

Appendix D: Photometric data used in the microlensing modelling

Photometric observations that were used in the microlensing model are shown in Table D.1. The complete table is available at the CDS.

Table D.1. Photometric follow-up observations of Gaia16aye used in the model.

HJD [d]	Magnitude [mag]	Error [mag]	Observatory code
2456961.36775	15.480	0.010	1
2456961.44175	15.480	0.010	1
2457068.91154	15.440	0.010	1
…	…	…	…
2457619.36442	14.350	0.009	2
2457623.42542	14.323	0.006	2
2457625.43582	14.320	0.006	2
…	…	…	…
2457612.33545	13.127	0.013	3
2457613.46778	12.894	0.003	3
2457614.40174	12.293	0.003	3
…	…	…	…
2457647.43662	14.256	0.007	4
2457648.33147	14.245	0.009	4
2457649.33125	12.208	0.004	4
…	…	…	…
2457690.67443	13.433	0.007	5
2457691.65978	13.433	0.006	5
2457692.59705	13.428	0.006	5
…	…	…	…
2457714.45266	12.246	0.003	6
2457714.46433	12.261	0.004	6
2457714.47873	12.280	0.005	6
…	…	…	…
2457610.28565	13.379	0.007	7
2457611.30428	13.286	0.005	7
2457616.35217	14.400	0.010	7
…	…	…	…
2457467.10912	17.020	0.170	8
2457489.03978	17.940	0.330	8
2457512.02932	18.110	0.290	8
…	…	…	…

Notes. Observatory codes: 1 *Gaia* (*G*), 2 Bialkow (*I*), 3 APT2 (*I*), 4 LT (*i*), 5 DEMONEXT (*I*), 6 Swarthmore (*I*), 7 UBT60 (*I*), and 8 ASAS-SN (*V*). The full data set is available at the CDS.